Author Manuscript

Performance of cloud 3D solvers in ice cloud shortwave radiation closure over the equatorial western Pacific Ocean

Tong Ren[1], Ping Yang[1,2,3], Jian Wei[2], Xianglei Huang[4], and Huiyan Sang[5]

[1] Department of Atmospheric Sciences, Texas A&M University, College Station, TX
[2] Department of Oceanography, Texas A&M University, College Station, TX
[3] Department of Physics & Astronomy, Texas A&M University, College Station, TX
[4] Department of Climate and Space Sciences and Engineering, University of Michigan, Ann Arbor, MI
[5] Department of Statistics, Texas A&M University, College Station, TX

Corresponding author: Tong Ren (tr7585@tamu.edu)

Key Points:

- Compared to accurate satellite cloud albedo observations, four tested fast computational methods overestimate the albedo.
- Three methods, treating cloud unevenness and horizontal reflections between clouds, reduce the overestimates by about 25%.
- Further improved estimates require data of cloud layer bases and tops, which may be provided by future satellite instruments.

This is the author manuscript accepted for publication and has undergone full peer review but has not been through the copyediting, typesetting, pagination and proofreading process, which may lead to differences between this version and the Version of Record. Please cite this article as doi: 10.1029/2021MS002754.

This article is protected by copyright. All rights reserved.

Author Manuscript

Abstract

For retrieving cloud optical properties from satellite images or computing these properties from climate model output, computationally efficient treatments of cloud horizontal inhomogeneity include the Monte Carlo Independent Column Approximation (McICA) and the Tripleclouds method. Computationally efficient treatment of cloud horizontal radiation exchanges includes the SPeedy Algorithm for Radiative TrAnsfer through CloUd Sides (SPARTACUS). As a test to derive properties from satellite images, we collocate Moderate Resolution Imaging Spectroradiometer (MODIS) cloud retrievals with near-nadir Cloud and the Earth's Radiant Energy System (CERES) footprints in July 2008 over an equatorial western Pacific Ocean region to compare the performance of the McICA, Tripleclouds, and SPARTACUS solvers to the conventional plane-parallel homogeneous (PPH) treatment. PPH overestimates cloud albedo, and the three solvers effectively reduce overestimation with root mean square error (RMSE) of shortwave upwelling irradiance decreasing between 15.72 and 18.53 W m^{-2}, or about 22 to 25%. Although cloud top variability does not get fed into the simulations, all three solvers also reduce the effect of cloud top variability on cloud albedo. Entrapment (energy reflected downward from clouds) and horizontal radiation transfer have opposite effects on the SPARTACUS cloud albedo simulation. The net effect depends on the cloud vertical extent, the unawareness of which limits the performance of the SPARTACUS solver.

Plain Language Summary

Light transfer calculations involving clouds are important because clouds reflect sunlight to space (a cooling effect) and also trap energy emitted below the clouds (a warming effect). A major question in climate studies is whether the cooling or warming effects are dominant in various climate scenarios. Models often simplify cloud calculations by assuming flat uniform clouds and ignoring horizontal light transfer between clouds, which overstates cloud cooling effects on climate. This study uses a month of satellite cloud images to compare the simplified method with three improved computational methods that consider cloud unevenness and horizontal light reflections. Compared to the simplified method, all three fast methods effectively reduce the overly high cloud reflection of sunlight. Though the new methods do not fully describe cloud unevenness, the new methods more realistically account for effects of cloud top unevenness on the reflection of sunlight, such as light absorbed by sunlit sides of clouds or shading of one cloud by another.

1 Introduction

The spatial resolution of general circulation models (GCMs) has become finer as computing power has increased. Early GCM horizontal resolution was around 5° to 10° from the late 1960s to the 1980s (e.g., Hansen et al., 1983; Manabe, 1969; Manabe & Wetherald, 1975), around 0.5° in the late 2000s (e.g., Zhao et al., 2009), and around 0.25° or even higher in recent GCMs (e.g., Chen & Lin, 2011; Haarsma et al., 2016; Harris & Lin, 2014; Small et al., 2014). Some global cloud-resolving GCMs can be run for short simulation periods with spatial resolutions of less than 5 km (Sato et al., 2009; Stevens et al., 2019). The need of increased model resolution stems from various research interests, such as interactions of large-scale atmospheric circulations with deep convection (Kuang et al., 2005), and seasonal predictions of tropical cyclones (e.g., Chen & Lin, 2011) and the Madden-Julian oscillation (MJO; e.g., Miura et al., 2007). However, the lack

This article is protected by copyright. All rights reserved.

of theoretical understanding of the complex atmospheric flows at the convection-permitting scale limits the performance improvement of higher-resolution models (Yano et al. 2018).

Parameterizations developed for coarse resolution models cannot be applied to fine resolution models through simple "extrapolation" (Yano et al., 2018). The conventional parameterization is the one-dimensional (1D) atmospheric radiation scheme. The 1D scheme is based on the plane-parallel homogenous (PPH) approximation, which assumes that a cloud is homogeneous within the cloudy part of each model layer. In a 3D atmosphere, vertical radiation fluxes are affected by cloud horizontal inhomogeneity and horizontal radiation exchanges inside the cloud and across cloud sides, which, however, are not considered in the 1D PPH approximation. Here, the effects on vertical radiation fluxes of horizontal cloud inhomogeneity and horizontal radiation transfer are referred to as the plane-parallel bias and the 3D effect, respectively. As the resolution of a GCM increases, the assumption of horizontal homogeneity of clouds generally improves (Boutle et al., 2014; Hill et al., 2015; Hogan & Illingworth, 2003). However, the 3D effect becomes more significant in higher resolution models, particularly when the ratio of cloud vertical extent to horizontal extent is not small (Gu & Liou, 2001).

For solving 3D radiative transfer, the Monte Carlo (MC) method (e.g., Cahalan et al., 2005; Davies, 1978) and the spherical harmonics discrete ordinate method (SHDOM; Evans, 1998) were introduced. MC and SHDOM are frequently used as benchmark 3D radiative transfer models, at least in some specific conditions (e.g., Barker et al., 2015; Villefranque et al., 2021). Comparisons of 3D and 1D PPH radiative transfer models show differences in the simulated radiative effects of typical clouds (e.g., Barker, 1994; Barker & Davies, 1992; Cahalan et al., 1994a,b). Introducing cloud horizontal variations typically changes cloud radiative effects in the shortwave (SW) and longwave (LW) by 10%, substantially changing the climate of a model (Shonk et al., 2012). However, accurate MC and SHDOM models are computationally costly (Pincus & Evans, 2009) and hence are not suitable for GCMs. However, a number of computationally efficient treatments of cloud horizontal inhomogeneity based on 1D radiative transfer solutions have been developed for practical applications.

Examples of better known 1D approximations include (1) scaling cloud bulk properties to a radiatively equivalent PPH cloud (e.g., Cahalan et al., 1994a; Oreopoulos & Davies, 1998), (2) the Gamma-weighted two stream method (Barker, 1996; Barker et al., 1996; Oreopoulos & Barker, 1999), (3) the MC Independent Column Approximation (McICA; Pincus et al., 2003, 2006) method that simultaneously samples the cloud state and spectral region, and (4) the "Tripleclouds" method (Shonk & Hogan, 2008). In the Tripleclouds method, each GCM grid box (horizontal area and vertical layer) is partitioned into three optically distinct regions, clear sky and optically thinner and optically thicker clouds. Specific locations of the three regions in each grid box are not specified. The optically thinner and thicker cloudy regions are assumed to be homogeneous within their own respective regions; the cloud water content (CWC) in each region is set to one standard deviation below and above the mean of the CWC distribution, respectively (Shonk & Hogan, 2010; Shonk et al., 2010). Such a setting keeps the first and second moments of the CWC distribution the same in the simplified two homogeneous cloudy regions but does not work when the CWC standard deviation exceeds the mean. Hence, the partition of CWC into the two cloudy regions has been modified in the latest Tripleclouds solver to include clouds that have extreme water content variations (Hogan et al., 2019). The Tripleclouds method also has been adapted to the two-stream solver (Meador & Weaver, 1980) in an efficient way (Shonk &

This article is protected by copyright. All rights reserved.

Author Manuscript

Hogan, 2008). However, notwithstanding the variety of available fast methods of handling cloud horizontal inhomogeneity, to the best of our knowledge, the practical fast treatment of horizontal radiation exchanges was not available until recently (Hogan & Shonk, 2013).

Solar radiation may escape from the side of clouds at high solar elevations and enter the side of clouds at low solar elevations (Barker et al., 2016; Loeb et al., 1997; Várnai & Davies, 1999; Zuidema & Evans, 1998). As a result, neglecting horizontal radiation transfer overestimates cloud reflectance when the sun is high and underestimates cloud reflectance when the sun is low (Pincus et al., 2005). Through adding extra terms to the two-stream differential equations to represent lateral exchange between regions, Hogan & Shonk (2013) introduced an efficient way to include effects on vertical radiation fluxes due to radiation interception by and leakage from cloud sides. The lateral exchange rate in Hogan & Shonk (2013) is assumed to be proportional to the normalized cloud perimeter length (L_c; unit: m^{-1}), which is defined as the ratio of the total cloud edge length in the horizontal plane in a model layer to the area of the selected domain. Some empirical approaches to estimate L_c have been suggested (Fielding et al., 2020; Hogan et al., 2018; Schäfer et al., 2016). The method developed in Hogan & Shonk (2013) was later called the SPeedy Algorithm for Radiative TrAnsfer through CloUd Sides (SPARTACUS), after some further improvements were made, including (1) extending the method to include SW and LW (Schäfer et al., 2016); and (2) facilitating horizontal radiation exchange calculations in the Tripleclouds framework (Hogan et al., 2016). Both the Tripleclouds and SPARTACUS solvers were added to the European Centre for Medium-Range Weather Forecasts (ECMWF) radiation scheme *ecRad* (Hogan & Bozzo, 2018). In the latest SPARTACUS solver, options include specification of entrapment (upward emitted energy from the surface and below clouds that is reflected downward by the clouds) (Hogan et al., 2019). The Tripleclouds and SPARTACUS solvers have been evaluated against more accurate radiative transfer calculations for cloud fields from large eddy simulations, reanalysis data, and active remote sensing observations (Hogan et al., 2016; Shonk & Hogan, 2008, 2010; Villefranque et al., 2021). However, GCM simulated cloud radiative effects (CREs) are often compared with satellite estimates (Dolinar et al., 2015; Wang & Su, 2013), where cloud bulk optical properties are retrieved from passive sensor observations (Minnis et al., 2011, 2020). To the best of our knowledge, it remains unclear how the Tripleclouds and SPARTACUS solvers perform, if the solvers are driven by retrieved cloud properties from passive sensors that cannot resolve the cloud vertical structure.

From the earliest use of passive-sensor-based bispectral cloud retrieval methods, it was known that the PPH assumption causes biases in retrieved cloud properties (e.g., Coakley & Davies, 1986; Pincus et al., 1995; Várnai & Marshak, 2001, 2007). Except for stratiform clouds when the solar zenith angle (θ_s) is < 60°, all water clouds over global oceans are substantially different from PPH clouds (Di Girolamo et al., 2010). Problems due to the PPH assumption are frequently reported when multi-angle passive observations are used to retrieve cloud properties (Horváth & Davies, 2004; Liang et al., 2009, 2015; Wang et al., 2018; Zuidema et al., 2003). The uneven structure of cloud tops causes cloud slopes that face toward or away from the sun to be brightly illuminated or shadowed, respectively. The solar reflectance and retrieved cloud optical thickness (COT, or τ) of the illuminated portions are significantly higher than from the shadowed portions of a cloud field, particularly when the sun is low (Várnai & Marshak, 2002). When $\theta_s >$ 40°, τ retrievals from near-nadir views are significantly smaller than retrievals from backscattering angles and larger than retrievals from forward-scattering directions (Liang & Girolamo, 2013). Kato & Marshak (2009) studied τ retrieval errors introduced by ignoring

This article is protected by copyright. All rights reserved.

Author Manuscript

subpixel and pixel-by-pixel cloud variability versus the solar and viewing geometric configuration. In addition, neglecting pixel-by-pixel cloud inhomogeneity in broken cumulus clouds can result in overly large cloud particle effective radius (CER, or r_{eff}) retrievals (Marshak et al., 2006). Due to subpixel cloud water variability, Moderate Resolution Imaging Spectroradiometer (MODIS) r_{eff} retrievals using 2.1 μm channel observations are systematically greater than from 3.7 μm channel observations (Zhang & Platnick, 2011; Zhang et al., 2012). Theoretical work has been done to quantify retrieval biases of τ and r_{eff} due to subpixel variability in both visible and shortwave-infrared observations (Zhang et al., 2016).

When erroneous passive τ and r_{eff} retrievals due to the PPH assumption are used in 1D broadband radiation flux calculations, the radiation fluxes are also biased (Kato et al., 2006). Knowing the influence of the 3D effect on passive sensor retrievals of cloud properties, this study focuses on addressing the question: *How do the Tripleclouds and SPARTACUS solvers perform in radiation closure, if passive sensor retrievals of cloud properties are used to drive the solvers?* While the LW cloud 3D effect is also not negligible (e.g., Pomroy & Illingworth, 2000; Schäfer et al., 2016), we focus on testing the performance of the two solvers in SW radiation closure. In addition, because the McICA has been widely used in the GCM community for its computational efficiency, we also include the McICA solver in our *ecRad* simulations for a comparison. Section 2 introduces the data and methods adopted in the test of the two solvers. Results and discussions are presented in section 3. Finally, conclusions are drawn in section 4.

2 Data and methods

2.1 The area of interest and data sources

The gradients of in-cloud radiative heating/cooling and horizontal heating between cloudy and clear-sky regions are thought to be important in anvil dynamics over the tropics (Dinh et al., 2010; Durran et al., 2009; Hartmann & Berry, 2017; Hartmann et al., 2018; Sokol & Hartmann, 2020; Wall et al., 2020). Hence, the lifecycle of tropical anvil clouds may be shaped by horizontal radiation transport within the clouds and between the clouds and the surrounding clear sky. We therefore test the cloud 3D solvers over the equatorial western Pacific Ocean from 0° to 12°N and 150°E to 170°E, an Intertropical Convergence Zone region where deep convection and anvil clouds prevail. This study uses nadir measurements from MODIS and the Cloud and the Earth's Radiant Energy System (CERES) on the Aqua satellite over the study area in July 2008 in the radiation closure experiment (so solar zenith angle θ_s ranges from 20.27 to 31.98°). Ice cloud properties in the radiation calculations use MODIS Collection 6 (MC6) Level 2 retrievals (Platnick et al., 2017). Measurements of the SW upwelling irradiance at the top of the atmosphere (TOA) F_{SW} are taken from the CERES Single Satellite Footprint (SSF) Level 2 Ed4A data (Loeb et al., 2016; Su et al., 2015b). Figure 1 shows a tropical deep convective system captured by MODIS over the study area in the local afternoon of 11 July 2008. In agreement with Ren et al. (2021), thin cirrus clouds at the edges of this convective system show smaller r_{eff}, and deep convective cores within the system show the largest τ.

The width of the CERES footprint (or field of view) ranges from 20 km at nadir to 70 km at oblique instrument viewing angles (Kato et al., 2005). Let θ_C be the CERES zenith angle and r_0 = 10 km be the radius of a CERES near-nadir ($\theta_C \leq 10°$) footprint (Zhan & Davies, 2016). As in Zhan & Davies (2016), the MC6 Level 2 1-km spatial resolution cloud retrievals are collocated

This article is protected by copyright. All rights reserved.

with near-nadir CERES footprints ($\theta_C \leq 10°$) from the same orbit by assigning each CERES near-nadir footprint to the MODIS 1-km pixels that have distances $\leq r_0$ from the center of this CERES footprint. The collocated footprints that have ice clouds only are kept for the radiation calculations, and footprints with liquid clouds or no clouds are discarded. In total, 5382 collocated CERES footprints are retained out of 21493 potential collocations. For each selected CERES footprint, with ice cloud properties from the collocated MODIS retrievals, the homogeneous, McICA, Tripleclouds, and SPARTACUS solvers in *ecRad* 1.4.0 are used to perform the radiation calculations. The homogeneous solver homogenizes cloud properties across the entire gridbox, rather than just homogenizing in the cloudy fraction of each layer. In practice, the homogeneous solver is called twice for clear and cloudy columns first, and then the mean F_{SW} is derived using the cloud fraction (f_c) as the weight. The arithmetic mean τ from the MODIS retrievals within each CERES footprint is used to drive the *ecRad* runs. The r_{eff} horizontal variation has a smaller impact on the cloud SW albedo bias than does the τ horizontal variation (Oreopoulos et al., 2007). For each selected CERES footprint, the τ-weighted mean r_{eff} is used for the *ecRad* runs. In a case study, Iwabuchi et al. (2014) showed that the extinction-weighted mean r_{eff} in a cloud column agrees better with an infrared-based passive retrieval of r_{eff} than r_{eff} at cloud top. Thus, with the mean τ and τ-weighted mean r_{eff} as input parameters, the homogeneous solver performs the PPH calculations. The F_{SW} calculations from the three solvers are compared with the CERES SSF F_{SW} retrievals (Loeb et al., 2001) that are widely used in radiation budget studies (Su et al., 2015b). Su et al. (2015a) estimated 9 W m^{-2} averaged instantaneous uncertainty of CERES F_{SW} over ocean under all-sky conditions. However, although CERES F_{SW} shows generally smaller uncertainties over thick overcast cloud scenes than over broken thin cloud scenes, uncertainty estimates are not reported for specific cloud types in Su et al. (2015a).

The fractional standard deviation of τ (f_σ), the ratio of the standard deviation to the mean of τ, is a required input parameter to the McICA, Tripleclouds, and SPARTACUS solvers. We calculate f_σ for each selected CERES footprint using the collocated MODIS τ retrievals. As in Kato et al. (2005), the cloud fraction (f_c) of each selected CERES footprint is approximated by the number of cloudy MODIS pixels divided by the total number of collocated MODIS pixels in this footprint. Such an estimation of f_c assumes that all MODIS cloudy pixels are overcast. In addition, radiative transfer calculations are sensitive to the selected ice cloud parameterization (e.g., Yi et al., 2017a,b). Loeb et al. (2018) suggest that the same ice cloud optical parameterization scheme be adopted in both satellite retrievals of ice cloud properties and broadband radiation flux calculations, if the retrieved optical properties are used to describe the ice cloud in the radiation calculations. In our *ecRad* runs, ice COT and CER are taken from MC6 retrievals, where ice particles are assumed to be aggregates of eight surface roughened hexagonal columns that follow a gamma size distribution with an effective variance of 0.1 (Platnick et al., 2017). This MC6 ice cloud optical scheme for both SW (Ren et al., 2020b) and LW (Kuo et al., 2020) has been added to the Rapid Radiative Transfer Model for GCM applications (RRTMG; Iacono et al., 2008; Mlawer et al., 1997). Because the current atmospheric gas radiative property scheme in *ecRad* is taken from RRTMG, the solar and terrestrial spectral band partitions are the same in the two models. Therefore, we straightforwardly incorporate the MC6 ice cloud scheme in RRTMG into *ecRad* for the present radiation calculations.

In the *ecRad* runs, the atmospheric conditions are obtained from the ECMWF atmospheric reanalysis, version 5 (ERA5; Hersbach et al., 2020), including hourly surface skin temperature,

This article is protected by copyright. All rights reserved.

Author Manuscript

and vertical pressure level profiles of geopotential, specific humidity, ozone mass mixing ratio, and temperature. Values at Aqua satellite overpass times are obtained using linear interpolation. The ERA5 data in the gridbox nearest to the center of each selected CERES footprint are used for the *ecRad* calculations. All 37 ERA5 pressure levels from 1 to 1000 hPa are used, including 7 levels between 100 and 250 hPa with an increment of 25 hPa. Therefore, the TOA is at 1 hPa in the *ecRad* simulations. As in previous studies (Kuo et al., 2017; Ren et al., 2020a), the volume mixing ratios of CO_2, N_2O, and CH_4 are set to 390.5, 0.3242, and 1.803 ppmv, respectively, the global mean values from the Fifth Assessment Report of the Intergovernmental Panel on Climate Change (Myhre et al., 2014). The average of the July 2008 daily means of Naval Research Laboratory's total solar irradiance version 2 (NRLTSI2; Coddington et al., 2016), 1360.60 W m^{-2}, is used to drive the *ecRad* runs. The SW ocean surface albedo is assumed to be spectrally independent and is from the CERES SSF data (Jin et al., 2004, 2011). Aerosols are not specified in the *ecRad* simulations.

2.2 A directional heterogeneity index for cloud top variability

In addition to cloud internal heterogeneity, cloud top variability also contributes to the cloud 3D effect (Iwabuchi & Hayasaka, 2002; Loeb et al., 1998; Várnai & Davies, 1999; Várnai & Marshak, 2003). The description of cloud top variability does not get fed into *ecRad*, but is useful for subsequent interpretation of the results. A useful quantity to describe cloud internal heterogeneity is f_σ, the fractional standard deviation of τ (Liang et al., 2009), and as previously mentioned, it is an *ecRad* input parameter. Because horizontal radiation transfer between adjacent cloudy pixels has less influence on the outgoing radiation in LW than in SW, the local brightness temperature gradient along the solar azimuth angle (φ_s) is used to quantify the cloud top variability (Várnai & Marshak, 2002). Inspired by this approach, with cloud top height (CTH or h) retrievals available at 1-km spatial resolution in MC6 (Baum et al., 2012), we calculate the spatial distribution of the h gradient along the horizontal direction of incident sunlight over each CERES footprint. Figure 2a shows the collocated MODIS h distribution over a selected CERES footprint in the middle of the study area in the local afternoon of 11 July 2008. In this case, h is as low as ~8 km in the northwestern portion and as high as ~14 km in the southeastern portion of the footprint, resulting in a positive h gradient along the northwest-to-southeast direction. Let $\partial h/\partial x$ and $\partial h/\partial y$ be the derivatives of h with respect to distance in the eastward and northward directions, respectively. As illustrated in Figures 2b and 2c, we first calculate the h gradient in the horizontal plane using the central difference for each collocated MODIS 1-km pixel within the CERES footprint:

$$\nabla h = \left(\frac{\partial h}{\partial x}, \frac{\partial h}{\partial y}\right). \quad (1)$$

Let **s** be the horizontal direction of incident sunlight, satisfying

$$\mathbf{s} = (\sin(\varphi_s + \pi), \cos(\varphi_s + \pi)). \quad (2)$$

Then, the h gradient along **s**, or $\mathbf{s} \cdot \nabla h$, is computed for each MODIS pixel (Figure 2d). In Figure 2d, the positive and negative $\mathbf{s} \cdot \nabla h$ areas may be regarded as illuminated and shadowed cloud top areas, respectively. We call the standard deviation of $\mathbf{s} \cdot \nabla h$ within each CERES footprint the directional heterogeneity index (DHI), which is used to quantify cloud top variability in this study. The correlations between the solver performance and f_σ and between the solver performance and DHI are analyzed.

2.3 The *ecRad* experiments

This article is protected by copyright. All rights reserved.

Author Manuscript

Deep convective clouds often have τ retrievals that exceed the upper bound of the look-up-table in the retrieval algorithm. Hence, only the anvil-like CERES footprints are adopted in our *ecRad* simulations. Radiation simulations are sensitive to assumed cloud vertical extent and vertical variation of r_{eff}. Therefore, in addition to the Control experiment, we also perform four additional experiments, where the cloud vertical extent and r_{eff} vertical variation are perturbed. Table 1 documents all *ecRad* experiments. Readers are referred to the Appendix for further details.

3 Results

Figure 3 shows the scatterplots of CERES F_{SW} vs. F_{SW} calculations from each of the four *ecRad* solvers in the Control experiment. The results show that all the *ecRad* simulations systematically overestimate the CERES F_{SW} (Figure 3), but the biases are almost exactly linear. It should be noted that the SPARTACUS solver is used with three regions at each height and hence its description of cloud structure is identical to Tripleclouds. In other words, both the horizontal radiation exchanges between clear-sky and cloudy regions and between optically thinner and thicker cloudy regions are included in the SPARTACUS runs. As shown in Figure 3 (also see Tables 3 and 4), compared to the homogeneous solver, both the McICA and Tripleclouds solvers significantly reduce the F_{SW} overestimation with RMSE decreasing from 72.7 (about 16% of the average F_{SW}) to 57.0 and 54.2 W m^{-2}, respectively, in the Control experiment. The result suggests that both the McICA and Tripleclouds solvers effectively reduce the positive cloud albedo bias of the homogeneous solver by roughly 25%. However, the Tripleclouds and SPARTACUS solvers show almost identical RMSEs, suggesting that the complete overlap of vertically adjacent cloud layers makes the explicit entrapment treatment in SPARTACUS less effective. We expect that the explicit entrapment in SPARTACUS will lead to a further reduced SW albedo for a high sun if cloud vertical extent can be known and properly set in the SPARTACUS simulation. The McICA and Tripleclouds solvers appear to be 7 times as fast as the SPARTACUS solver in our experiments (Table 2).

Cloud 3D effects likely only explain part of the albedo bias shown in Figure 3. Passive τ and r_{eff} retrievals that agree with the sensor radiance may not match the radiance angular distribution (Kato et al., 2006), which may explain a large portion of the F_{SW} bias in Figure 3. In addition to the angular distribution, the wavelength dependence of the radiation (e.g., in the near-IR) could also be a source of error, particularly when passive r_{eff} retrievals are biased. Moreover, the two-stream assumption in *ecRad* may explain some of the F_{SW} bias (Barker et al., 2015). Indeed, the 1D PPH assumption in the MODIS cloud retrievals also contributes to the root mean square errors (RMSEs) of F_{SW} in Figure 3. The selected near-nadir ($\theta_C \leq 10°$) anvil-like samples in the *ecRad* experiments have solar zenith angles ranging from 20.27° to 31.98°, so all collocated MODIS pixels are viewed by the instrument from the backscatter directions. Although spaceborne imaging spectroradiometers tend to underestimate f_c due to their finite resolution that does not detect small or thin clouds (Dutta et al., 2020; Zhao & Di Girolamo, 2006), the f_c bias effect on F_{SW} estimation is small (Ham et al., 2019). Hence, the assumed overcast MODIS 1-km cloudy pixels are not likely to explain the F_{SW} overestimation in this study.

Let δ_{Homo}, δ_{Mc}, δ_{Tri}, and δ_{SPA} be the relative errors of the F_{SW} calculations from the four different solvers, satisfying

$$\delta_{\text{Homo}} = \left(F_{\text{SW,Homo}} - F_{\text{SW,CERES}}\right)/F_{\text{SW,CERES}}, \quad (3)$$

$$\delta_{\text{Mc}} = \left(F_{\text{SW,Mc}} - F_{\text{SW,CERES}}\right)/F_{\text{SW,CERES}}, \quad (4)$$

This article is protected by copyright. All rights reserved.

Author Manuscript

$$\delta_{\mathrm{Tri}} = \left(F_{\mathrm{SW,Tri}} - F_{\mathrm{SW,CERES}}\right)/F_{\mathrm{SW,CERES}}, \quad (5)$$

$$\delta_{\mathrm{SPA}} = \left(F_{\mathrm{SW,SPA}} - F_{\mathrm{SW,CERES}}\right)/F_{\mathrm{SW,CERES}}, \quad (6)$$

where $F_{\mathrm{SW,CERES}}$ is the CERES F_{SW} and $F_{\mathrm{SW,Homo}}$, $F_{\mathrm{SW,Mc}}$, $F_{\mathrm{SW,Tri}}$, and $F_{\mathrm{SW,SPA}}$ are the F_{SW} calculations from the four solvers, respectively. As shown in Figures 4a and 5a, δ_{Homo} shows a weak positive correlation with the square root of f_c and a weak negative correlation with $\log_{10}$(DHI). The positive correlation suggests that the F_{SW} overestimation by the homogeneous solver increases slightly with increasing cloud water horizontal variability. The negative correlation suggests that the F_{SW} overestimation by the homogeneous solver decreases slightly with increasing cloud top variability. The results strongly agree with Várnai & Davies (1999). Through 3D Monte Carlo simulations, Várnai and Davies (1999) suggest that cloud internal variability tends to move radiation from thicker to thinner regions, resulting in a decreased cloud albedo, whereas cloud top variability tends to move radiation from thinner to thicker regions, resulting in an increased cloud albedo. In Figure 4, the correlation coefficient is largest in the homogeneous run, which suggests that the albedo overestimation due to cloud horizontal inhomogeneity is effectively reduced in all the three 3D solvers. In Figure 5, the correlation coefficient is most negative in the homogeneous run, less negative with the other three 3D solvers, and least negative in the McICA run. The result suggests that including cloud internal variability in the 3D solvers also reduces the impact of cloud top variability on the albedo bias. The correlation coefficients between δ_{Tri} and $\log_{10}$(DHI) and between δ_{SPA} and $\log_{10}$(DHI) are similar (Figures 5c and 5d), suggesting that the influence of cloud top variability on the albedo bias is not adequately represented in the Control SPARTACUS experiment design.

Figure 6 shows that the improvement of the Tripleclouds solver relative to the homogeneous solver increases with the degree of cloud horizontal inhomogeneity. Although a number of samples have larger Tripleclouds solver absolute percentage errors ($|\delta_{\mathrm{Tri}}|$) than homogeneous solver absolute percentage errors ($|\delta_{\mathrm{Homo}}|$), the difference in the absolute percentage error between the two solvers ($|\delta_{\mathrm{Tri}}|$-$|\delta_{\mathrm{Homo}}|$) is generally more negative when the cloud is more horizontally inhomogeneous. Tables 3 and 4 document the RMSEs and mean absolute percentage errors (MAPEs) of F_{SW} calculations in the *ecRad* experiments. The Thin and Thick experiments show higher and lower RMSEs and MAPEs than the Control experiment, respectively. Given the same τ, thinner clouds have larger extinction coefficients and hence are more reflective than thicker clouds. While the SPARTACUS simulations show slightly higher RMSEs than the Tripleclouds simulations in the Control and Thick experiments, the SPARTACUS simulation shows a slightly lower RMSE than the Tripleclouds simulation in the Thin experiment (Table 3). The result suggests that entrapment and radiation exchanges through cloud sides have opposite effects on the cloud albedo. The net effect depends on the cloud vertical extent. Thicker clouds have larger side areas and hence can intercept more radiation than thinner clouds. The SPARTACUS simulations have slightly lower MAPEs than the Tripleclouds simulations in all experiments (Table 4). Compared to the Control experiment, both the EOF1 and EOF2 experiments show increased RMSEs and MAPEs. Given the same τ, clouds with smaller r_{eff} are more reflective than with larger r_{eff}. The upper portion of the cloud layer has a smaller r_{eff} in the EOF1 experiment than in the Control experiment (Figure A2b); r_{eff} is smaller in the EOF2 experiment than in the Control experiment in almost the entire cloud layer (Figure A2c).

4 Conclusions

This article is protected by copyright. All rights reserved.

Author Manuscript

As GCM resolution has increased, the cloud 3D effect becomes more significant. By depicting cloudy layers as partly optically thin and thick, the Tripleclouds solver was developed for computationally efficient inhomogeneity treatment. Through solving the horizontal radiation exchange rate between two optically distinct regions, a computationally efficient horizontal radiation flux treatment, SPARTACUS, was introduced. Both the Tripleclouds and SPARTACUS solvers are included in the ECMWF radiation scheme *ecRad*. In addition to GCM use, 3D radiative solvers also have offline applications. For example, offline radiation calculations are needed to derive cloud radiative effects in the atmosphere and at the surface (Kato et al., 2018; 2019), the GCM simulations of which are of interest (e.g., Wild et al., 2019). In the derivation of the cloud radiative effects, cloud optical properties are often retrieved using passive sensors that cannot resolve cloud vertical structures. This study is the first to extensively evaluate the Tripleclouds and SPARTACUS solvers using collocated passive sensor cloud property retrievals. Aqua MC6 Level 2 1-km pixels are collocated with CERES near-nadir footprints in July 2008 over an equatorial Pacific Ocean region. The *ecRad* 1.4.0 scheme is used to perform radiation calculations for individual selected CERES anvil-like ice cloud footprints with input cloud parameters from MODIS retrievals. The calculations are performed four times to compare the conventional homogeneous, McICA, Tripleclouds, and SPARTACUS solvers. The McICA solver, a computationally efficient 3D solver, has been widely used in current GCMs. The resultant upward shortwave radiation fluxes at the top of the atmosphere are compared with the CERES counterparts. To quantify cloud top variability, we calculate the cloud top height (h) gradient along the horizontal direction of incident sunlight at each MODIS pixel in every selected CERES footprint. The standard deviation of h gradients within each CERES footprint is named the directional heterogeneity index (DHI).

Overall, all the *ecRad* simulations overestimate the cloud albedo, primarily due to the ice optical parameterization. Because passive cloud optical thickness (τ) and effective radius (r_{eff}) retrievals are based on the radiance measurements in the sensor viewing direction, the retrieved τ and r_{eff} often vary across the radiance angular distribution (Kato et al., 2006), although the same ice optical parameterization is assumed in passive cloud property retrievals and broadband radiative flux calculations. In addition, the two-stream assumption in *ecRad* may explain some of the cloud albedo overestimation (Barker et al., 2015). Further theoretical studies involving 3D radiative transfer with realistic cloud fields (e.g., from large eddy simulation models) are really needed to gain more insight into the reason for the albedo overestimation. The McICA and Tripleclouds solvers appear to be 7 times faster than the SPARTACUS solver. In agreement with the previous study (Várnai & Davies, 1999), cloud albedo overestimation by the homogenous solver increases with increasing cloud internal variability but decreases with increasing cloud top variability. Relative to the homogeneous solver, the other three solvers all effectively reduce the TOA albedo overestimation from CERES-derived albedo of 36.80% to a range from 39.69 to 39.74%. Although cloud top variability is not fed into *ecRad*, the three 3D solvers also reduce the effect of cloud top variability on cloud albedo. The explicit entrapment treatment and horizontal radiation transfer through cloud sides in SPARTACUS have opposite effects on the cloud albedo. The net effect of the two processes is sensitive to the cloud vertical extent. One limitation is that passive sensors cannot resolve the cloud vertical structure, which must be assumed or obtained from another source when passive retrievals of cloud properties are used to drive the SPARTACUS solver. Cloud vertical structure can be more adequately represented if combined passive-active observations are used (Barker et al., 2011; Illingworth et al., 2015), but active sensors to date (cloud radars and lidars) do not observe a wide enough swath for daily

This article is protected by copyright. All rights reserved.

Author Manuscript

global coverage. On the other hand, when the 3D solvers are used in GCMs, parameterizations have to be applied to obtain the required descriptions of clouds for driving the solvers. Performance of the *ecRad* solvers may be different from this study, if only approximate descriptions of clouds that a GCM can provide are used to drive the solvers.

Appendix: Details in setting up the *ecRad* experiments

Based on aircraft cloud ice studies (Krämer et al., 2016), Ren et al. (2021) suggest that cold-top thin cirrus, anvil-like clouds, and deep convective cores over the equatorial western Pacific Ocean region can be separated using the combined passive-active satellite retrievals of τ and r_{eff} (Kato et al., 2010; 2011). The mean vertical extent of the anvil-like clouds averages 3.9 km with a small day-to-day variation (Ren et al., 2021). While the distribution of the logarithm of mean τ, or $\log_{10}(\tau)$, shows a heavy tail (positive skewness) over the selected CERES footprints (Figure A1b), the mean r_{eff} sample distribution appears to be symmetric (Figure A1a). Perhaps, the selected samples consist primarily of anvil-like clouds and deep convective cores; few samples are dominated by thin cirrus clouds. We assume that the $\log_{10}(\tau)$ samples are a mixture of two Gaussian distributions to separate the anvil-like clouds (Type I) from the deep convective cores (Type II). The two Gaussian distributions are then determined using the expectation–maximization (EM) algorithm (Scrucca et al., 2016) as in Ren et al. (2021), resulting in 4718 Type I and 664 Type II samples (Figure A1d). In addition, we take the logarithm of DHI to make it a more normal distribution (Figure A1c).

The Type II samples are not used in the *ecRad* runs, because the samples include MODIS τ retrievals that exceed the upper limit of the retrieval look-up-table. At present, it remains unclear what portion of a deep convective cloud contributes to a passive sensor retrieved τ. Based on 3D Monte Carlo simulations, Forster et al. (2021) argue that passive sensor observed radiance is not sensitive to the detailed water distribution within the in-cloud region beyond a certain distance from the cloud boundary along the line of sight. In the *ecRad* runs of the Type I samples, we assume vertically homogeneous clouds with a fixed vertical extent of 3.9 km (Ren et al. 2021) and CTHs being the means from the collocated MODIS pixels. In other words, τ in each model layer is proportional to the cloud vertical extent in this layer. Then, τ in each model layer is converted to the in-cloud ice mass mixing ratio (q_i) as follows:

$$q_i = \frac{2[q/(1-q)+\varepsilon]r_{\text{eff}}\tau\rho_{ice}R_{\text{d}}T}{3\varepsilon pL}. \quad \text{(A1)}$$

In the above equation, q is specific humidity; R_{d} = 287.04 J K^{-1} kg^{-1} is the gas constant for dry air; ε = 0.622 is the ratio of R_{d} to the gas constant for water vapor (R_{v} = 461.5 J K^{-1} kg^{-1}); ρ_{ice} = 916.7 kg m^{-3} is the density of solid ice; T is temperature; p is pressure; and L is thickness of the model layer. Note that the input parameter ice cloud mass mixing ratio to *ecRad* is a gridbox mean quantity, i.e., the product of q_i and f_c (Tiedtke, 1996). Cloud fraction f_c is assumed to be constant in all cloudy model layers. While the day-to-day mean top height variation of anvil-like clouds is small, the mean base height shows a day-to-day standard deviation of 1.4 km (Ren et al. 2021). To test the sensitivity of *ecRad* simulations to cloud vertical extent, we perform another two *ecRad* experiments, where the cloud vertical extents are set to one cloud base height standard deviation below and above the cloud vertical extent in the Control experiment (2.5 and 5.3 km), respectively. We call the two experiments Thin and Thick.

This article is protected by copyright. All rights reserved.

In our *ecRad* Control experiment, all model layers are assumed to have the same r_{eff}. However, the outgoing solar radiation is influenced by the vertical variation of r_{eff} (Zhang et al., 2010). Using combined MODIS and CloudSat measurements of global marine water clouds, Saito et al. (2018) derived the first two leading empirical orthogonal functions (EOFs) of the droplet size profile in a 6-layer normalized τ space. The first two EOFs can explain 94% of the droplet size profile variability (Saito et al., 2018). Because we have not found reported anvil-like cloud r_{eff} vertical distribution statistics in previous studies, we adopt the two EOFs in Saito et al. (2018) to test the sensitivity of the *ecRad* calculations to the vertical variation of r_{eff}. In reality, anvil-like cloud r_{eff} profiles may be very different from those of marine liquid clouds. Two more experiments are conducted, where the r_{eff} vertical distributions in cloudy model layers are scaled using the two EOFs, respectively. We call the two experiments EOF1 and EOF2. The MODIS retrieved r_{eff} generally represents r_{eff} at an optical depth between 0.2 and 0.4 of the total τ (Nakajima & King, 1990). Therefore, in experiments EOF1 and EOF2, the τ-weighted r_{eff} is assumed to represent r_{eff} in the second layer (from the top) in the 6-layer normalized τ space. Then, with the determined r_{eff} in all 6 layers in the normalized τ space, r_{eff} in every *ecRad* cloud model layer is obtained using spline interpolation. In agreement with previous studies (Saito et al., 2017; van Diedenhoven et al., 2020), low-altitude ice clouds generally have larger particle sizes than high-altitude ice clouds (Figure A2). In the EOF1 experiment, r_{eff} increases from cloud top to cloud base (Figure A2b). In the EOF2 experiment, from cloud top to cloud base, r_{eff} first increases and then decreases (Figure A2c).

In addition, the normalized cloud perimeter length L_c is a required parameter for running the SPARTACUS solver. Due to the fractal nature of a cloud perimeter (Lovejoy, 1982) and the uncertainty of cloud fraction (or f_c) observations (Di Girolamo & Davies, 1997; Pincus et al., 1999), instead of directly estimating L_c from the collocated MODIS cloud image, we parameterize L_c in all cloud model layers as follows:

$$\begin{cases} L_c = \frac{2\sqrt{1-f_c}}{r_0}, 0.5 < f_c \le 1 \\ L_c = \frac{2\sqrt{f_c}}{r_0}, \qquad f_c \le 0.5 \end{cases}. \tag{A2}$$

As shown in Figure A3, the L_c parameterization in Eq. (A2) assumes that anvil-like clouds tend to aggregate. This parameterization is not meant to be suitable for all types of clouds in GCM applications, where a careful analysis of observations is required (Fielding et al. 2020). Because passive cloud retrievals cannot provide information about the cloud vertical structure, in the *ecRad* experiments, the cloud overlap decorrelation length (ODL; Hogan & Illingworth, 2000, 2003) is set to a very large value of 10^6 m. Otherwise, with f_c being assumed to be constant in all cloudy model layers, the lowered correlation between vertically adjacent cloud layers will result in a total cloud fraction larger than the constant f_c. In a previous radiation closure experiment, Kato et al. (2005) reported increased cloud albedo with an increased number of computational layers, due to difficulties in cloud overlap treatment.

Tables

Table 1 *The ecRad experiments.*

Experiment	Cloud vertical extent (km)	r_{eff}
Control	3.9	Vertically homogeneous
Thin	2.5	Vertically homogeneous

This article is protected by copyright. All rights reserved.

Thick	5.3	Vertically homogeneous
EOF1	3.9	EOF1 scaled (Saito et al. 2018)
EOF2	3.9	EOF2 scaled (Saito et al. 2018)

Table 2 *Times elapsed (s) in the radiative transfer computations of the three ecRad 3D solvers in the Control experiment.*

McICA	Tripleclouds	SPARTACUS
4.107	3.834	30.704

Table 3 *RMSEs (W m^{-2}) of F_{SW} calculations in the ecRad experiments.*

Experiment	Homogeneous	McICA	Tripleclouds	SPARTACUS
Control	72.74	57.02	54.21	54.27
Thin	73.56	57.74	55.01	54.93
Thick	71.74	56.48	53.25	53.45
EOF1	75.45	58.98	56.25	56.30
EOF2	75.84	59.70	57.01	57.04

Table 4 *Mean absolute percentage errors (MAPEs) of F_{SW} in the ecRad experiments.*

Experiment	Homogeneous	McICA	Tripleclouds	SPARTACUS
Control	13.10%	10.74%	10.33%	10.30%
Thin	13.32%	10.88%	10.53%	10.47%
Thick	12.83%	10.61%	10.09%	10.08%
EOF1	13.23%	10.84%	10.42%	10.39%
EOF2	13.75%	11.31%	10.92%	10.89%

Figure captions

Figure 1. (a) True color image composited from MODIS Level 1b bands 1 (red, 620–670 μm), 4 (green, 545–565 μm), and 3 (blue, 459–479 μm), (b) MODIS Level 2 ice COT, and (c) MODIS Level 2 ice CER (μm) of a tropical deep convective system over the study area 0° to 12°N and 150°E to 170°E in the local afternoon of 11 July 2008.

Figure 2. Distributions of collocated MODIS (a) h (km), (b) h gradient along the eastward direction (km km^{-1}), (c) h gradient along the northward direction (km km^{-1}), and (d) h gradient along the horizontal direction of incident sunlight (km km^{-1}) over a CERES footprint in the middle of the study area in the local afternoon of 11 July 2008. The black arrow in (d) marks the horizontal direction of incident sunlight.

Figure 3. Scatterplots of CERES F_{SW} vs. F_{SW} calculations from each of the four *ecRad* solvers in the Control experiment. RMSE = root mean square error.

Figure 4. Scatterplots of the F_{SW} relative error of each solver vs. the square root of f_σ in the Control experiment. In each panel, r is the correlation coefficient and p is the t-test p-value.

This article is protected by copyright. All rights reserved.

Author Manuscript

Figure 5. Scatterplots of the F_{SW} relative error of each solver vs. $\log_{10}$(DHI) in the Control experiment. In each panel, r is the correlation coefficient and p is the *t*-test p-value.

Figure 6. Scatterplot of $\Delta 13 = |\delta_{Tri}| - |\delta_{Homo}|$ vs. the square root of f_σ. The dashed black line is the linear regression fitted line; r is the correlation coefficient and p is the p-value.

Figure A1. Distributions of samples of (a) CER (μm), (b) log10(COT), (c) log10(DHI), and (d) log10(COT) for Type I and II clouds, respectively.

Figure A2. Vertical distributions of r_{eff} for all anvil-like (Type I) samples in the (a) Control, (b) EOF1, and (c) EOF2 *ecRad* experiments.

Figure A3. Schematic illustrating the L_c parameterization in Eq. (4). In each panel, the big circle represents a near-nadir CERES footprint with a radius of r_0; the gray and white regions in the circle represent the cloudy and cloud-free regions over the CERES footprint, respectively.

References

Barker, H. W. (1994). Solar radiative transfer for wind-sheared cumulus cloud fields. *Journal of Atmospheric Sciences, 51*(9), 1141-1156. https://doi.org/10.1175/1520-0469(1994)051<1141:SRTFWS>2.0.CO;2

Barker, H. W. (1996). A parameterization for computing grid-averaged solar fluxes for inhomogeneous marine boundary layer clouds. Part I: Methodology and homogeneous biases. *Journal of Atmospheric Sciences, 53*(16), 2289-2303. https://doi.org/10.1175/1520-0469(1996)053<2289:APFCGA>2.0.CO;2

Barker, H. W., & Davies, J. A. (1992). Solar radiative fluxes for stochastic, scale-invariant broken cloud fields. *Journal of the Atmospheric Sciences, 49*(13), 1115-1126. https://doi.org/10.1175/1520-0469(1992)049<1115:SRFFSS>2.0.CO;2

Barker, H. W., Wiellicki, B. A., & Parker, L. (1996). A parameterization for computing grid-averaged solar fluxes for inhomogeneous marine boundary layer clouds. Part II: Validation using satellite data. *Journal of Atmospheric Sciences, 53*(16), 2304-2316. https://doi.org/10.1175/1520-0469(1996)053<2304:APFCGA>2.0.CO;2

Barker, H. W., Cole, J. N., Li, J., & von Salzen, K. (2016). A parametrization of 3-D subgrid-scale clouds for conventional GCMs: Assessment using A-Train satellite data and solar radiative transfer characteristics. *Journal of Advances in Modeling Earth Systems, 8*(2), 566-597. https://doi.org/10.1002/2015MS000601

Barker, H. W., Cole, J. N., Li, J., Yi, B., & Yang, P. (2015). Estimation of errors in two-stream approximations of the solar radiative transfer equation for cloudy-sky conditions. *Journal of the Atmospheric Sciences, 72*(11), 4053-4074. https://doi.org/10.1175/JAS-D-15-0033.1

Barker, H. W., Jerg, M. P., Wehr, T., Kato, S., Donovan, D. P., & Hogan, R. J. (2011). A 3D cloud-construction algorithm for the EarthCARE satellite mission. *Quarterly Journal of the Royal Meteorological Society, 137*(657), 1042-1058. https://doi.org/10.1002/qj.824

Baum, B. A., Menzel, W. P., Frey, R. A., Tobin, D. C., Holz, R. E., Ackerman, S. A., et al. (2012). MODIS cloud-top property refinements for Collection 6. *Journal of Applied Meteorology and Climatology, 51*(6), 1145-1163. https://doi.org/10.1175/JAMC-D-11-0203.1

This article is protected by copyright. All rights reserved.

Author Manuscript

Boutle, I., Eyre, J., & Lock, A. (2014). Seamless stratocumulus simulation across the turbulent gray zone. *Monthly Weather Review, 142*(4), 1655-1668. https://doi.org/10.1175/MWR-D-13-00229.1

Cahalan, R. F., Oreopoulos, L., Marshak, A., Evans, K. F., Davis, A. B., Pincus, R., et al. (2005). The I3RC: Bringing together the most advanced radiative transfer tools for cloudy atmospheres. *Bulletin of the American Meteorological Society, 86*(9), 1275-1294. https://doi.org/10.1175/BAMS-86-9-1275

Cahalan, R. F., Ridgway, W., Wiscombe, W. J., Bell, T. L., & Snider, J. B. (1994a). The albedo of fractal stratocumulus clouds. *Journal of the Atmospheric Sciences, 51*(16), 2434-2455. https://doi.org/10.1175/1520-0469(1994)051<2434:TAOFSC>2.0.CO;2

Cahalan, R. F., Ridgway, W., Wiscombe, W. J., & Gollmer, S. (1994b). Independent pixel and Monte Carlo estimates of stratocumulus albedo. *Journal of the Atmospheric Sciences, 51*(24), 3776-3790. https://doi.org/10.1175/1520-0469(1994)051<3776:IPAMCE>2.0.CO;2Chen, J. H., & Lin, S. J. (2011). The remarkable predictability of inter-annual variability of Atlantic hurricanes during the past decade. *Geophysical Research Letters, 38*(11), L11804. https://doi.org/10.1029/2011GL047629

Coakley Jr, J. A., & Davies, R. (1986). The effect of cloud sides on reflected solar radiation as deduced from satellite observations. *Journal of Atmospheric Sciences, 43*(10), 1025-1035. https://doi.org/10.1175/1520-0469(1986)043<1025:TEOCSO>2.0.CO;2

Coddington, O., Lean, J., Pilewskie, P., Snow, M., & Lindholm, D. (2016). A solar irradiance climate data record. *Bulletin of the American Meteorological Society, 97*(7), 1265-1282. https://doi.org/10.1175/BAMS-D-14-00265.1

Davies, R. (1978). The effect of finite geometry on the three-dimensional transfer of solar irradiance in clouds. *Journal of the Atmospheric Sciences, 35*(9), 1712-1725. https://doi.org/10.1175/1520-0469(1978)035<1712:TEOFGO>2.0.CO;2

Di Girolamo, L., & Davies, R. (1997). Cloud fraction errors caused by finite resolution measurements. *Journal of Geophysical Research: Atmospheres, 102*(D2), 1739-1756. https://doi.org/10.1029/96JD02663

Di Girolamo, L., Liang, L., & Platnick, S. (2010). A global view of one-dimensional solar radiative transfer through oceanic water clouds. *Geophysical Research Letters, 37*(18), L18809. https://doi.org/10.1029/2010GL044094

Dinh, T. P., Durran, D., & Ackerman, T. (2010). Maintenance of tropical tropopause layer cirrus. *Journal of Geophysical Research: Atmospheres, 115*(D2), D02104. https://doi.org/10.1029/2009JD012735

Dolinar, E. K., Dong, X., Xi, B., Jiang, J. H., & Su, H. (2015). Evaluation of CMIP5 simulated clouds and TOA radiation budgets using NASA satellite observations. *Climate Dynamics, 44*(7-8), 2229-2247. https://doi.org/10.1007/s00382-014-2158-9

Durran, D. R., Dinh, T., Ammerman, M., & Ackerman, T. (2009). The mesoscale dynamics of thin tropical tropopause cirrus. *Journal of the Atmospheric Sciences, 66*(9), 2859-2873. https://doi.org/10.1175/2009JAS3046.1

Dutta, S., Di Girolamo, L., Dey, S., Zhan, Y., Moroney, C. M., & Zhao, G. (2020). The reduction in near-global cloud cover after correcting for biases caused by finite resolution measurements. *Geophysical Research Letters, 47*(23), e2020GL090313. https://doi.org/10.1029/2020GL090313

This article is protected by copyright. All rights reserved.

Evans, K. F. (1998). The spherical harmonics discrete ordinate method for three-dimensional atmospheric radiative transfer. *Journal of the Atmospheric Sciences, 55*(3), 429-446. https://doi.org/10.1175/1520-0469(1998)055<0429:TSHDOM>2.0.CO;2

Fielding, M. D., Schäfer, S. A., Hogan, R. J., & Forbes, R. M. (2020). Parametrizing cloud geometry and its application in a subgrid cloud-edge erosion scheme. *Quarterly Journal of the Royal Meteorological Society, 146*(729), 1651-1667. https://doi.org/ 10.1002/qj.3758

Forster, L., Davis, A. B., Diner, D. J., & Mayer, B. (2021). Toward cloud tomography from space using MISR and MODIS: locating the "Veiled Core" in opaque convective clouds. *Journal of the Atmospheric Sciences, 78*(1), 155-166. https://doi.org/10.1175/JAS-D-19-0262.1

Gu, Y., & Liou, K. (2001). Radiation parameterization for three-dimensional inhomogeneous cirrus clouds: Application to climate models. *Journal of Climate, 14*(11), 2443-2457.

Haarsma, R. J., Roberts, M. J., Vidale, P. L., Senior, C. A., Bellucci, A., Bao, Q., et al. (2016). High resolution model intercomparison project (HighResMIP v1. 0) for CMIP6. *Geoscientific Model Development, 9*(11), 4185-4208. https://doi.org/10.5194/gmd-9-4185-2016

Ham, S.-H., Kato, S., & Rose, F. G. (2019). Impacts of partly cloudy pixels on shortwave broadband irradiance computations. *Journal of Atmospheric and Oceanic Technology, 36*(3), 369-386. https://doi.org/10.1175/JTECH-D-18-0153.1

Hansen, J., Russell, G., Rind, D., Stone, P., Lacis, A., Lebedeff, S., et al. (1983). Efficient three-dimensional global models for climate studies: Models I and II. *Monthly Weather Review, 111*(4), 609-662. https://doi.org/10.1175/1520-0493(1983)111<0609:ETDGMF>2.0.CO;2

Harris, L. M., & Lin, S.-J. (2014). Global-to-regional nested grid climate simulations in the GFDL high resolution atmospheric model. *Journal of Climate, 27*(13), 4890-4910. https://doi.org/10.1175/JCLI-D-13-00596.1

Hartmann, D. L., & Berry, S. E. (2017). The balanced radiative effect of tropical anvil clouds. *Journal of Geophysical Research: Atmospheres, 122*(9), 5003-5020. https://doi.org/10.1002/2017JD026460

Hartmann, D. L., Gasparini, B., Berry, S. E., & Blossey, P. N. (2018). The life cycle and net radiative effect of tropical anvil clouds. *Journal of Advances in Modeling Earth Systems, 10*(12), 3012-3029. https://doi.org/10.1029/2018MS001484

Hersbach, H., Bell, B., Berrisford, P., Hirahara, S., Horányi, A., Muñoz-Sabater, J., et al. (2020). The ERA5 global reanalysis. *Quarterly Journal of the Royal Meteorological Society, 146*(730), 1999-2049. https://doi.org/10.1002/qj.3803

Hill, P., Morcrette, C., & Boutle, I. (2015). A regime-dependent parametrization of subgrid-scale cloud water content variability. *Quarterly Journal of the Royal Meteorological Society, 141*(691), 1975-1986. https://doi.org/10.1002/qj.2506

Hogan, R. J., & Bozzo, A. (2018). A flexible and efficient radiation scheme for the ECMWF model. *Journal of Advances in Modeling Earth Systems, 10*(8), 1990-2008. https://doi.org/10.1029/2018MS001364

Hogan, R. J., & Illingworth, A. J. (2000). Deriving cloud overlap statistics from radar. *Quarterly Journal of the Royal Meteorological Society, 126*(569), 2903-2909. https://doi.org/10.1002/qj.49712656914

Hogan, R. J., & Illingworth, A. J. (2003). Parameterizing ice cloud inhomogeneity and the overlap of inhomogeneities using cloud radar data. *Journal of the Atmospheric Sciences, 60*(5), 756-767. https://doi.org/10.1175/1520-0469(2003)060<0756:PICIAT>2.0.CO;2

This article is protected by copyright. All rights reserved.

Hogan, R. J., & Shonk, J. K. (2013). Incorporating the effects of 3D radiative transfer in the presence of clouds into two-stream multilayer radiation schemes. *Journal of the Atmospheric Sciences, 70*(2), 708-724. https://doi.org/10.1175/JAS-D-12-041.1

Hogan, R. J., Quaife, T., & Braghiere, R. (2018). Fast matrix treatment of 3-D radiative transfer in vegetation canopies: SPARTACUS-Vegetation 1.1. *Geoscientific Model Development, 11*(1), 339-350. https://doi.org/10.5194/gmd-11-339-2018

Hogan, R. J., Fielding, M. D., Barker, H. W., Villefranque, N., & Schäfer, S. A. (2019). Entrapment: An important mechanism to explain the shortwave 3D radiative effect of clouds. *Journal of the Atmospheric Sciences, 76*(7), 2123-2141. https://doi.org/10.1175/JAS-D-18-0366.1

Hogan, R. J., Schäfer, S. A., Klinger, C., Chiu, J. C., & Mayer, B. (2016). Representing 3-D cloud radiation effects in two-stream schemes: 2. Matrix formulation and broadband evaluation. *Journal of Geophysical Research: Atmospheres, 121*(14), 8583-8599. https://doi.org/10.1002/2016JD024875

Horváth, A., & Davies, R. (2004). Anisotropy of water cloud reflectance: A comparison of measurements and 1D theory. *Geophysical Research Letters, 31*(1), L01102. https://doi.org/10.1029/2003GL018386

Iacono, M. J., Delamere, J. S., Mlawer, E. J., Shephard, M. W., Clough, S. A., & Collins, W. D. (2008). Radiative forcing by long-lived greenhouse gases: Calculations with the AER radiative transfer models. *Journal of Geophysical Research: Atmospheres, 113*(D13), D13103. https://doi.org/10.1029/2008JD009944

Illingworth, A. J., Barker, H., Beljaars, A., Ceccaldi, M., Chepfer, H., Clerbaux, N., et al. (2015). The EarthCARE satellite: The next step forward in global measurements of clouds, aerosols, precipitation, and radiation. *Bulletin of the American Meteorological Society, 96*(8), 1311-1332. https://doi.org/10.1175/BAMS-D-12-00227.1

Iwabuchi, H., & Hayasaka, T. (2002). Effects of cloud horizontal inhomogeneity on the optical thickness retrieved from moderate-resolution satellite data. *Journal of the Atmospheric Sciences, 59*(14), 2227-2242. https://doi.org/10.1175/1520-0469(2002)059<2227:EOCHIO>2.0.CO;2

Iwabuchi, H., Yamada, S., Katagiri, S., Yang, P., & Okamoto, H. (2014). Radiative and microphysical properties of cirrus cloud inferred from infrared measurements made by the Moderate Resolution Imaging Spectroradiometer (MODIS). Part I: Retrieval method. *Journal of Applied Meteorology and Climatology, 53*(5), 1297-1316. https://doi.org/10.1175/JAMC-D-13-0215.1

Jin, Z., Charlock, T. P., Smith Jr, W. L., & Rutledge, K. (2004). A parameterization of ocean surface albedo. *Geophysical Research Letters, 31*(22), L22301. https://doi.org/10.1029/2004GL021180

Jin, Z., Qiao, Y., Wang, Y., Fang, Y., & Yi, W. (2011). A new parameterization of spectral and broadband ocean surface albedo. *Optics express, 19*(27), 26429-26443. https://doi.org/10.1364/OE.19.026429

Kato, S., & Marshak, A. (2009). Solar zenith and viewing geometry-dependent errors in satellite retrieved cloud optical thickness: Marine stratocumulus case. *Journal of Geophysical Research: Atmospheres, 114*(D1), D01202. https://doi.org/10.1029/2008JD010579

Kato, S., Hinkelman, L. M., & Cheng, A. (2006). Estimate of satellite-derived cloud optical thickness and effective radius errors and their effect on computed domain-averaged

This article is protected by copyright. All rights reserved.

irradiances. *Journal of Geophysical Research: Atmospheres, 111*(D17201). https://doi.org/10.1029/2005JD006668

Kato, S., Rose, F. G., & Charlock, T. P. (2005). Computation of domain-averaged irradiance using satellite-derived cloud properties. *Journal of Atmospheric and Oceanic Technology, 22*(2), 146-164. https://doi.org/10.1175/JTECH-1694.1

Kato, S., Sun-Mack, S., Miller, W. F., Rose, F. G., Chen, Y., Minnis, P., & Wielicki, B. A. (2010). Relationships among cloud occurrence frequency, overlap, and effective thickness derived from CALIPSO and CloudSat merged cloud vertical profiles. *Journal of Geophysical Research: Atmospheres, 115*(D4), D00H28. https://doi.org/10.1029/2009JD012277

Kato, S., Rose, F. G., Ham, S. H., Rutan, D. A., Radkevich, A., Caldwell, T. E., et al. (2019). Radiative heating rates computed with clouds derived from satellite-based passive and active sensors and their effects on generation of available potential energy. *Journal of Geophysical Research: Atmospheres, 124*(3), 1720-1740. https://doi.org/10.1029/2018JD028878

Kato, S., Rose, F. G., Rutan, D. A., Thorsen, T. J., Loeb, N. G., Doelling, D. R., et al. (2018). Surface irradiances of edition 4.0 Clouds and the Earth's Radiant Energy System (CERES) Energy Balanced and Filled (EBAF) data product. *Journal of Climate, 31*(11), 4501-4527. https://doi.org/10.1175/JCLI-D-17-0523.1

Kato, S., Rose, F. G., Sun-Mack, S., Miller, W. F., Chen, Y., Rutan, D. A., et al. (2011). Improvements of top-of-atmosphere and surface irradiance computations with CALIPSO-, CloudSat-, and MODIS-derived cloud and aerosol properties. *Journal of Geophysical Research: Atmospheres, 116*(D19), D19209. https://doi.org/10.1029/2011JD016050

Krämer, M., Rolf, C., Luebke, A., Afchine, A., Spelten, N., Costa, A., et al. (2016). A microphysics guide to cirrus clouds-Part 1: Cirrus types. *Atmospheric Chemistry and Physics, 16*, 3463-3483. https://doi.org/10.5194/acp-16-3463-2016

Kuang, Z., Blossey, P. N., & Bretherton, C. S. (2005). A new approach for 3D cloud-resolving simulations of large-scale atmospheric circulation. *Geophysical Research Letters, 32*(2), L02809. https://doi.org/10.1029/2004GL021024

Kuo, C.-P., Yang, P., Huang, X., Chen, Y.-H., & Liu, G. (2020). Assessing the accuracy and efficiency of longwave radiative transfer models involving scattering effect with cloud optical property parameterizations. *Journal of Quantitative Spectroscopy and Radiative Transfer, 240*, 106683. https://doi.org/10.1016/j.jqsrt.2019.106683

Kuo, C. P., Yang, P., Huang, X., Feldman, D., Flanner, M., Kuo, C., & Mlawer, E. J. (2017). Impact of multiple scattering on longwave radiative transfer involving clouds. *Journal of Advances in Modeling Earth Systems, 9*(8), 3082-3098. https://doi.org/10.1002/2017MS001117

Liang, L., & Girolamo, L. D. (2013). A global analysis on the view-angle dependence of plane-parallel oceanic liquid water cloud optical thickness using data synergy from MISR and MODIS. *Journal of Geophysical Research: Atmospheres, 118*(5), 2389-2403. https://doi.org/10.1029/2012JD018201

Liang, L., Di Girolamo, L., & Platnick, S. (2009). View-angle consistency in reflectance, optical thickness and spherical albedo of marine water-clouds over the northeastern Pacific through MISR-MODIS fusion. *Geophysical Research Letters, 36*(9), L09811. https://doi.org/10.1029/2008GL037124

Liang, L., Di Girolamo, L., & Sun, W. (2015). Bias in MODIS cloud drop effective radius for oceanic water clouds as deduced from optical thickness variability across scattering angles.

This article is protected by copyright. All rights reserved.

Author Manuscript

Journal of Geophysical Research: Atmospheres, *120*(15), 7661-7681. https://doi.org/10.1002/2015JD023256

Loeb, N. G., Várnai, T., & Davies, R. (1997). Effect of cloud inhomogeneities on the solar zenith angle dependence of nadir reflectance. *Journal of Geophysical Research: Atmospheres*, *102*(D8), 9387-9395. https://doi.org/10.1029/96JD03719

Loeb, N. G., Várnai, T., & Winker, D. M. (1998). Influence of subpixel-scale cloud-top structure on reflectances from overcast stratiform cloud layers. *Journal of the Atmospheric Sciences*, *55*(18), 2960-2973. https://doi.org/10.1175/1520-0469(1998)055<2960:IOSSCT>2.0.CO;2

Loeb, N. G., Manalo-Smith, N., Su, W., Shankar, M., & Thomas, S. (2016). CERES top-of-atmosphere Earth radiation budget climate data record: Accounting for in-orbit changes in instrument calibration. *Remote Sensing*, *8*(3), 182. https://doi.org/10.3390/rs8030182

Loeb, N. G., Priestley, K. J., Kratz, D. P., Geier, E. B., Green, R. N., Wielicki, B. A., et al. (2001). Determination of unfiltered radiances from the Clouds and the Earth's Radiant Energy System instrument. *Journal of Applied Meteorology*, *40*(4), 822-835. https://doi.org/10.1175/1520-0450(2001)040<0822:DOURFT>2.0.CO;2

Loeb, N. G., Yang, P., Rose, F. G., Hong, G., Sun-Mack, S., Minnis, P., et al. (2018). Impact of ice cloud microphysics on satellite cloud retrievals and broadband flux radiative transfer model calculations. *Journal of Climate*, *31*(5), 1851-1864. https://doi.org/10.1175/JCLI-D-17-0426.1

Lovejoy, S. (1982). Area-perimeter relation for rain and cloud areas. *Science*, *216*(4542), 185-187. https://doi.org/10.1126/science.216.4542.185

Manabe, S. (1969). Climate and the ocean circulation: I. The atmospheric circulation and the hydrology of the earth's surface. *Monthly Weather Review*, *97*(11), 739-774. https://doi.org/10.1175/1520-0493(1969)097%3C0739:CATOC%3E2.3.CO;2

Manabe, S., & Wetherald, R. T. (1975). The effects of doubling the CO2 concentration on the climate of a general circulation model. *Journal of the Atmospheric Sciences*, *32*(1), 3-15. https://doi.org/10.1175/1520-0469(1975)032<0003:TEODTC>2.0.CO;2

Marshak, A., Platnick, S., Várnai, T., Wen, G., & Cahalan, R. F. (2006). Impact of three-dimensional radiative effects on satellite retrievals of cloud droplet sizes. *Journal of Geophysical Research: Atmospheres*, *111*(D9), D09207. https://doi.org/10.1029/2005JD006686

Meador, W., & Weaver, W. (1980). Two-stream approximations to radiative transfer in planetary atmospheres: A unified description of existing methods and a new improvement. *Journal of the Atmospheric Sciences*, *37*(3), 630-643. https://doi.org/10.1175/1520-0469(1980)037<0630:TSATRT>2.0.CO;2

Minnis, P., Sun-Mack, S., Chen, Y., Chang, F.-L., Yost, C. R., Smith, W. L., et al. (2020). CERES MODIS Cloud Product Retrievals for Edition 4—Part I: Algorithm changes. *IEEE Transactions on Geoscience and Remote Sensing*, *59*(4), 2744-2780. https://doi.org/10.1109/TGRS.2020.3008866

Minnis, P., Sun-Mack, S., Young, D. F., Heck, P. W., Garber, D. P., Chen, Y., et al. (2011). CERES Edition-2 cloud property retrievals using TRMM VIRS and Terra and Aqua MODIS data—Part I: Algorithms. *IEEE Transactions on Geoscience and Remote Sensing*, *49*(11), 4374-4400. https://doi.org/10.1109/TGRS.2011.2144601

Miura, H., Satoh, M., Nasuno, T., Noda, A. T., & Oouchi, K. (2007). A Madden-Julian oscillation event realistically simulated by a global cloud-resolving model. *Science*, *318*(5857), 1763-1765. https://doi.org/10.1126/science.1148443

This article is protected by copyright. All rights reserved.

Author Manuscript

Mlawer, E. J., Taubman, S. J., Brown, P. D., Iacono, M. J., & Clough, S. A. (1997). Radiative transfer for inhomogeneous atmospheres: RRTM, a validated correlated-k model for the longwave. *Journal of Geophysical Research: Atmospheres, 102*(D14), 16663-16682. https://doi.org/10.1029/97JD00237

Myhre, G., Shindell, D., & Pongratz, J. (2014). *Anthropogenic and natural radiative forcing* (1107415322). Retrieved from Cambridge, U. K., and New York:

Nakajima, T., & King, M. D. (1990). Determination of the optical thickness and effective particle radius of clouds from reflected solar radiation measurements. Part I: Theory. *Journal of the Atmospheric Sciences, 47*(15), 1878-1893. https://doi.org/10.1175/1520-0469(1990)047<1878:DOTOTA>2.0.CO;2

Oreopoulos, L., & Barker, H. W. (1999). Accounting for subgrid-scale cloud variability in a multi-layer 1D solar radiative transfer algorithm. *Quarterly Journal of the Royal Meteorological Society, 125*(553), 301-330.

Oreopoulos, L., & Davies, R. (1998). Plane parallel albedo biases from satellite observations. Part II: Parameterizations for bias removal. *Journal of Climate, 11*(5), 933-944. https://doi.org/10.1175/1520-0442(1998)011<0933:PPABFS>2.0.CO;2

Oreopoulos, L., Cahalan, R. F., & Platnick, S. (2007). The plane-parallel albedo bias of liquid clouds from MODIS observations. *Journal of Climate, 20*(20), 5114-5125. https://doi.org/10.1175/JCLI4305.1

Pincus, R., & Evans, K. F. (2009). Computational cost and accuracy in calculating three-dimensional radiative transfer: Results for new implementations of Monte Carlo and SHDOM. *Journal of the Atmospheric Sciences, 66*(10), 3131-3146. https://doi.org/10.1175/2009JAS3137.1

Pincus, R., Barker, H. W., & Morcrette, J. J. (2003). A fast, flexible, approximate technique for computing radiative transfer in inhomogeneous cloud fields. *Journal of Geophysical Research: Atmospheres, 108*(D13), 4376. https://doi.org/10.1029/2002JD003322

Pincus, R., Hannay, C., & Evans, K. F. (2005). The accuracy of determining three-dimensional radiative transfer effects in cumulus clouds using ground-based profiling instruments. *Journal of the Atmospheric Sciences, 62*(7), 2284-2293. https://doi.org/10.1175/JAS3464.1

Pincus, R., Hemler, R., & Klein, S. A. (2006). Using stochastically generated subcolumns to represent cloud structure in a large-scale model. *Monthly Weather Review, 134*(12), 3644-3656. https://doi.org/10.1175/MWR3257.1

Pincus, R., McFarlane, S. A., & Klein, S. A. (1999). Albedo bias and the horizontal variability of clouds in subtropical marine boundary layers: Observations from ships and satellites. *Journal of Geophysical Research: Atmospheres, 104*(D6), 6183-6191. https://doi.org/10.1029/1998JD200125

Pincus, R., Szczodrak, M., Gu, J., & Austin, P. (1995). Uncertainty in cloud optical depth estimates made from satellite radiance measurements. *Journal of Climate, 8*(5), 1453-1462. https://doi.org/10.1175/1520-0442(1995)008<1453:UICODE>2.0.CO;2

Platnick, S., Meyer, K. G., King, M. D., Wind, G., Amarasinghe, N., Marchant, B., et al. (2017). The MODIS cloud optical and microphysical products: Collection 6 updates and examples from Terra and Aqua. *IEEE Transactions on Geoscience and Remote Sensing, 55*(1), 502-525. https://doi.org/10.1109/TGRS.2016.2610522

Pomroy, H. R., & Illingworth, A. J. (2000). Ice cloud inhomogeneity: Quantifying bias in emissivity from radar observations. *Geophysical Research Letters, 27*(14), 2101-2104. https://doi.org/10.1029/1999GL011149

This article is protected by copyright. All rights reserved.

Author Manuscript

Ren, T., Li, D., Muller, J., & Yang, P. (2021). Sensitivity of radiative flux simulations to ice cloud parameterization over the equatorial western Pacific Ocean region. *Journal of the Atmospheric Sciences, 78*(8), 2549-2571. https://doi.org/10.1175/JAS-D-21-0017.1

Ren, T., Yang, P., Schumacher, C., Huang, X., & Lin, W. (2020a). Impact of cloud longwave scattering on radiative fluxes associated with the Madden-Julian Oscillation in the Indian Ocean and Maritime Continent. *Journal of Geophysical Research: Atmospheres, 125*(13), e2020JD032591. https://doi.org/10.1029/2020JD032591

Ren, T., Yang, P., Tang, G., Huang, X., & Mlawer, E. (2020b). Improved δ-Eddington approximation for optically thin clouds. *Journal of Quantitative Spectroscopy and Radiative Transfer, 240*, 106694. https://doi.org/10.1016/j.jqsrt.2019.106694

Saito, M., Iwabuchi, H., Yang, P., Tang, G., King, M. D., & Sekiguchi, M. (2017). Ice particle morphology and microphysical properties of cirrus clouds inferred from combined CALIOP-IIR measurements. *Journal of Geophysical Research: Atmospheres, 122*(8), 4440-4462. https://doi.org/10.1002/2016JD026080

Saito, M., Yang, P., Hu, Y., Liu, X., Loeb, N., Smith Jr, W. L., & Minnis, P. (2018). An efficient method for microphysical property retrievals in vertically inhomogeneous marine water clouds using MODIS–CloudSat measurements. *Journal of Geophysical Research: Atmospheres, 124*(4), 2174-2193. https://doi.org/10.1029/2018JD029659

Sato, T., Miura, H., Satoh, M., Takayabu, Y. N., & Wang, Y. (2009). Diurnal cycle of precipitation in the tropics simulated in a global cloud-resolving model. *Journal of Climate, 22*(18), 4809-4826. https://doi.org/10.1175/2009JCLI2890.1

Schäfer, S. A., Hogan, R. J., Klinger, C., Chiu, J. C., & Mayer, B. (2016). Representing 3-D cloud radiation effects in two-stream schemes: 1. Longwave considerations and effective cloud edge length. *Journal of Geophysical Research: Atmospheres, 121*(14), 8567-8582. https://doi.org/10.1002/2016JD024876

Scrucca, L., Fop, M., Murphy, T. B., & Raftery, A. E. (2016). mclust 5: clustering, classification and density estimation using Gaussian finite mixture models. *The R journal, 8*(1), 289-317.

Shonk, J. K., & Hogan, R. J. (2008). Tripleclouds: An efficient method for representing horizontal cloud inhomogeneity in 1D radiation schemes by using three regions at each height. *Journal of Climate, 21*(11), 2352-2370. https://doi.org/10.1175/2007JCLI1940.1

Shonk, J. K., & Hogan, R. J. (2010). Effect of improving representation of horizontal and vertical cloud structure on the Earth's global radiation budget. Part II: The global effects. *Quarterly Journal of the Royal Meteorological Society, 136*(650), 1205-1215. https://doi.org/10.1002/qj.646

Shonk, J. K., Hogan, R. J., & Manners, J. (2012). Impact of improved representation of horizontal and vertical cloud structure in a climate model. *Climate Dynamics, 38*(11-12), 2365-2376. https://doi.org/10.1007/s00382-011-1174-2

Shonk, J. K., Hogan, R. J., Edwards, J. M., & Mace, G. G. (2010). Effect of improving representation of horizontal and vertical cloud structure on the Earth's global radiation budget. Part I: Review and parametrization. *Quarterly Journal of the Royal Meteorological Society, 136*(650), 1191-1204. https://doi.org/10.1002/qj.647

Small, R. J., Bacmeister, J., Bailey, D., Baker, A., Bishop, S., Bryan, F., et al. (2014). A new synoptic scale resolving global climate simulation using the Community Earth System Model. *Journal of Advances in Modeling Earth Systems, 6*(4), 1065-1094. https://doi.org/10.1002/2014MS000363

This article is protected by copyright. All rights reserved.

Author Manuscript

Sokol, A. B., & Hartmann, D. L. (2020). Tropical anvil clouds: Radiative driving towards a preferred state. *Journal of Geophysical Research: Atmospheres, 125*(21), e2020JD033107. https://doi.org/10.1029/2020JD033107

Stevens, B., Satoh, M., Auger, L., Biercamp, J., Bretherton, C. S., Chen, X., et al. (2019). DYAMOND: the DYnamics of the Atmospheric general circulation Modeled On Non-hydrostatic Domains. *Progress in Earth and Planetary Science, 6*(1), 1-17. https://doi.org/10.1186/s40645-019-0304-z

Su, W., Corbett, J., Eitzen, Z., & Liang, L. (2015a). Next-generation angular distribution models for top-of-atmosphere radiative flux calculation from CERES instruments: Validation. *Atmospheric Measurement Techniques, 8*(8), 3297-3313. https://doi.org/10.5194/amt-8-3297-2015

Su, W., Corbett, J., Eitzen, Z., & Liang, L. (2015b). Next-generation angular distribution models for top-of-atmosphere radiative flux calculation from CERES instruments: Methodology. *Atmospheric Measurement Techniques, 8*(2), 611-632. https://doi.org/10.5194/amt-8-611-2015

Tiedtke, M. (1996). An extension of cloud-radiation parameterization in the ECMWF model: The representation of subgrid-scale variations of optical depth. *Monthly Weather Review, 124*(4), 745-750. https://doi.org/10.1175/1520-0493(1996)124<0745:AEOCRP>2.0.CO;2

van Diedenhoven, B., Ackerman, A. S., Fridlind, A. M., Cairns, B., & Riedi, J. (2020). Global statistics of ice microphysical and optical properties at tops of optically thick ice clouds. *Journal of Geophysical Research: Atmospheres, 125*(6), e2019JD031811. https://doi.org/10.1029/2019JD031811

Várnai, T., & Davies, R. (1999). Effects of cloud heterogeneities on shortwave radiation: Comparison of cloud-top variability and internal heterogeneity. *Journal of the Atmospheric Sciences, 56*(24), 4206-4224. https://doi.org/10.1175/1520-0469(1999)056<4206:EOCHOS>2.0.CO;2

Várnai, T., & Marshak, A. (2001). Statistical analysis of the uncertainties in cloud optical depth retrievals caused by three-dimensional radiative effects. *Journal of the Atmospheric Sciences, 58*(12), 1540-1548. https://doi.org/10.1175/1520-0469(2001)058<1540:SAOTUI>2.0.CO;2

Várnai, T., & Marshak, A. (2002). Observations of three-dimensional radiative effects that influence MODIS cloud optical thickness retrievals. *Journal of the Atmospheric Sciences, 59*(9), 1607-1618. https://doi.org/10.1016/j.jqsrt.2009.06.013

Várnai, T., & Marshak, A. (2003). A method for analyzing how various parts of clouds influence each other's brightness. *Journal of Geophysical Research: Atmospheres, 108*(D22), 4706. https://doi.org/10.1029/2003JD003561

Várnai, T., & Marshak, A. (2007). View angle dependence of cloud optical thicknesses retrieved by Moderate Resolution Imaging Spectroradiometer (MODIS). *Journal of Geophysical Research: Atmospheres, 112*(D6), D06203. https://doi.org/10.1029/2005JD006912

Villefranque, N., Blanco, S., Couvreux, F., Fournier, R., Gautrais, J., Hogan, R. J., et al. (2021). Process-based climate model development harnessing machine learning: III. The representation of cumulus geometry and their 3D radiative effects. *Journal of Advances in Modeling Earth Systems, 13*(4), e2020MS002423. https://doi.org/10.1029/2020MS002423

Wall, C. J., Norris, J. R., Gasparini, B., Smith Jr, W. L., Thieman, M. M., & Sourdeval, O. (2020). Observational evidence that radiative heating modifies the life cycle of tropical anvil clouds. *Journal of Climate, 33*(20), 8621-8640. https://doi.org/10.1175/JCLI-D-20-0204.1

This article is protected by copyright. All rights reserved.

Wang, H., & Su, W. (2013). Evaluating and understanding top of the atmosphere cloud radiative effects in Intergovernmental Panel on Climate Change (IPCC) Fifth Assessment Report (AR5) Coupled Model Intercomparison Project Phase 5 (CMIP5) models using satellite observations. *Journal of Geophysical Research: Atmospheres, 118*(2), 683-699. https://doi.org/10.1029/2012JD018619

Wang, Y., Hioki, S., Yang, P., King, M., Di Girolamo, L., Fu, D., & Baum, B. (2018). Inference of an Optimal Ice Particle Model through Latitudinal Analysis of MISR and MODIS Data. *Remote Sensing, 10*(12), 1981. https://doi.org/10.3390/rs10121981

Wild, M., Hakuba, M. Z., Folini, D., Dörig-Ott, P., Schär, C., Kato, S., & Long, C. N. (2019). The cloud-free global energy balance and inferred cloud radiative effects: an assessment based on direct observations and climate models. *Climate Dynamics, 52*(7), 4787-4812. https://doi.org/10.1007/s00382-018-4413-y

Yano, J.-I., Ziemiański, M. Z., Cullen, M., Termonia, P., Onvlee, J., Bengtsson, L., et al. (2018). Scientific challenges of convective-scale numerical weather prediction. *Bulletin of the American Meteorological Society, 99*(4), 699-710. https://doi.org/10.1175/BAMS-D-17-0125.1

Yi, B., Rapp, A. D., Yang, P., Baum, B. A., & King, M. D. (2017a). A comparison of Aqua MODIS ice and liquid water cloud physical and optical properties between Collection 6 and Collection 5.1: Pixel-to-pixel comparisons. *Journal of Geophysical Research: Atmospheres, 122*(8), 4528-4549. https://doi.org/10.1002/2016JD025586

Yi, B., Rapp, A. D., Yang, P., Baum, B. A., & King, M. D. (2017b). A comparison of Aqua MODIS ice and liquid water cloud physical and optical properties between Collection 6 and Collection 5.1: Cloud radiative effects. *Journal of Geophysical Research: Atmospheres, 122*(8), 4550-4564. https://doi.org/10.1002/2016JD025654

Zhan, Y., & Davies, R. (2016). Intercalibration of CERES, MODIS, and MISR reflected solar radiation and its application to albedo trends. *Journal of Geophysical Research: Atmospheres, 121*(11), 6273-6283. https://doi.org/10.1002/2016JD025073

Zhang, Z., & Platnick, S. (2011). An assessment of differences between cloud effective particle radius retrievals for marine water clouds from three MODIS spectral bands. *Journal of Geophysical Research: Atmospheres, 116*(D20), D20215. https://doi.org/10.1029/2011JD016216

Zhang, Z., Platnick, S., Yang, P., Heidinger, A. K., & Comstock, J. M. (2010). Effects of ice particle size vertical inhomogeneity on the passive remote sensing of ice clouds. *Journal of Geophysical Research: Atmospheres, 115*(D17), D17203. https://doi.org/10.1029/2010JD013835

Zhang, Z., Ackerman, A. S., Feingold, G., Platnick, S., Pincus, R., & Xue, H. (2012). Effects of cloud horizontal inhomogeneity and drizzle on remote sensing of cloud droplet effective radius: Case studies based on large-eddy simulations. *Journal of Geophysical Research: Atmospheres, 117*(D19), D19208. https://doi.org/10.1029/2012JD017655

Zhang, Z., Werner, F., Cho, H. M., Wind, G., Platnick, S., Ackerman, A., et al. (2016). A framework based on 2-D Taylor expansion for quantifying the impacts of subpixel reflectance variance and covariance on cloud optical thickness and effective radius retrievals based on the bispectral method. *Journal of Geophysical Research: Atmospheres, 121*(12), 7007-7025. https://doi.org/10.1002/2016JD024837

This article is protected by copyright. All rights reserved.

Zhao, G., & Di Girolamo, L. (2006). Cloud fraction errors for trade wind cumuli from EOS-Terra instruments. *Geophysical Research Letters, 33*(20), L20802. https://doi.org/10.1029/2006GL027088

Zhao, M., Held, I. M., Lin, S.-J., & Vecchi, G. A. (2009). Simulations of global hurricane climatology, interannual variability, and response to global warming using a 50-km resolution GCM. *Journal of Climate, 22*(24), 6653-6678. https://doi.org/10.1175/2009JCLI3049.1

Zuidema, P., & Evans, K. F. (1998). On the validity of the independent pixel approximation for boundary layer clouds observed during ASTEX. *Journal of Geophysical Research: Atmospheres, 103*(D6), 6059-6074. https://doi.org/10.1029/98JD00080

Zuidema, P., Davies, R., & Moroney, C. (2003). On the angular radiance closure of tropical cumulus congestus clouds observed by the Multiangle Imaging Spectroradiometer. *Journal of Geophysical Research: Atmospheres, 108*(D20), 4626. https://doi.org/10.1029/2003JD003401

Acknowledgments

This study was supported by the Department of Energy under Grant DE-SC0019278 via a subaward (SUBK00009230) from the University of Michigan to Texas A&M University. We thank Steven Schroeder, who helped edit the manuscript. We thank Robin Hogan and two anonymous reviewers for their in-depth and constructive comments on this study. P. Yang also acknowledges the support by the endowment funds related to the David Bullock Harris Chair in Geosciences at Texas A&M University (02-512231-10000). The *ecRad* experiments in this study were performed using Texas A&M High Performance Research Computing facilities.

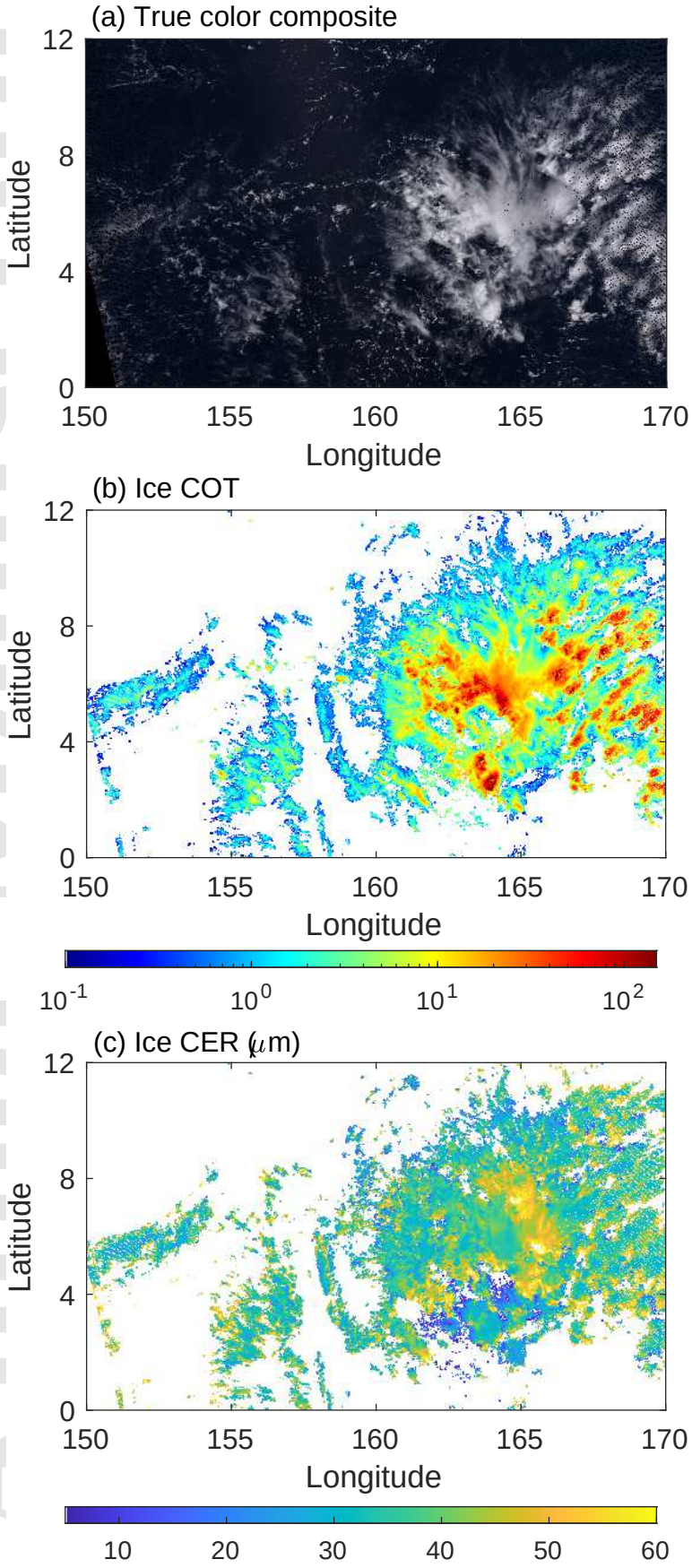
Data Availability Statement

The Aqua MODIS Collection 6 Level 1b (MYD021KM and MYD03) and Level 2 cloud (MYD06) data were downloaded from NASA's Level-1 and Atmosphere Archive and Distribution System (LAADS) Distributed Active Archive Center (DAAC) at https://ladsweb.modaps.eosdis.nasa.gov. The CERES SSF level 2 Ed4A data were accessed from NASA Langley Research Center at https://ceres.larc.nasa.gov/data/#ssf-level-2. The *ecRad* 1.4.0 solver was obtained from https://github.com/ecmwf/ecrad. The ERA5 data were accessed from the Climate Data Store at https://cds.climate.copernicus.eu. The daily mean NRLTSI2 data were downloaded from the LASP's Interactive Solar Irradiance Data Center server at https://lasp.colorado.edu/lisird/data/nrl2_tsi_P1D.

This article is protected by copyright. All rights reserved.

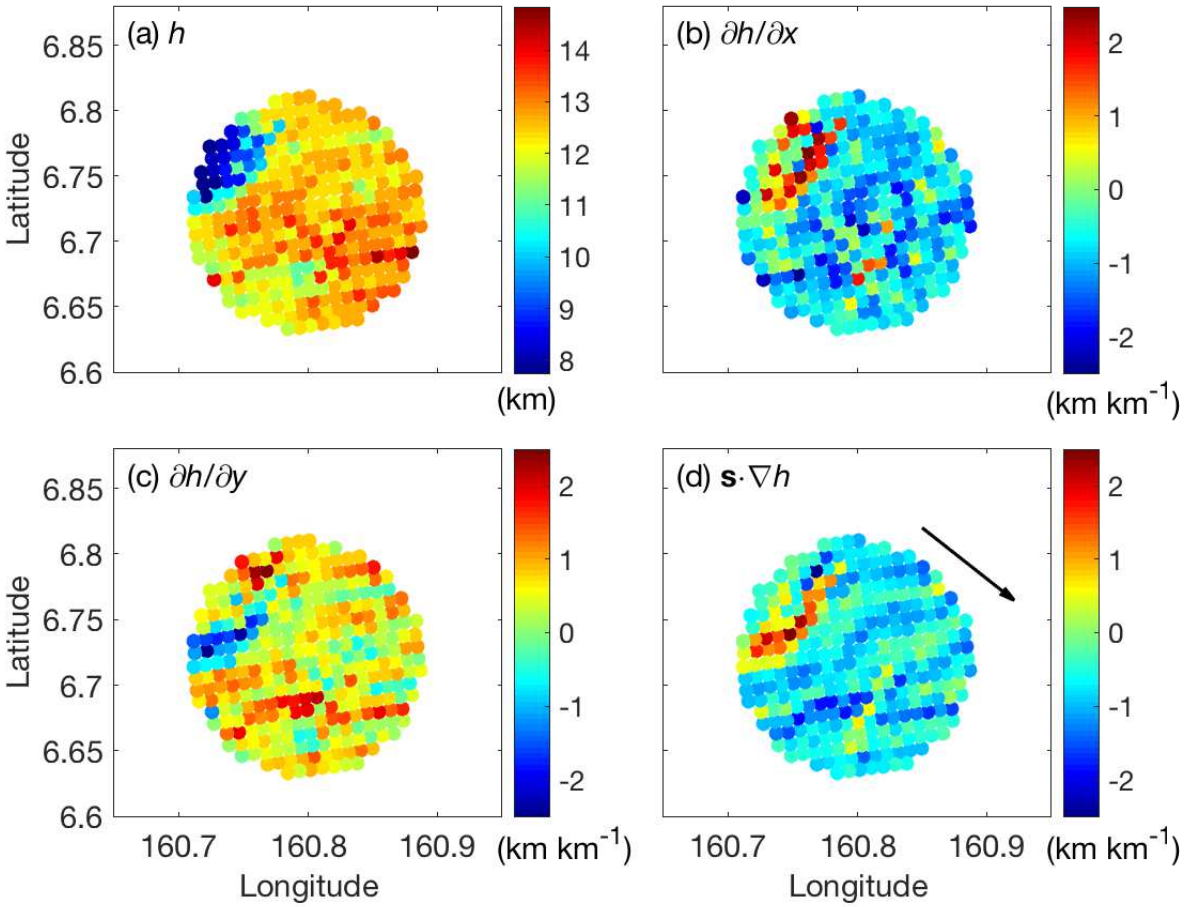
Author Manuscript

Author Manuscript

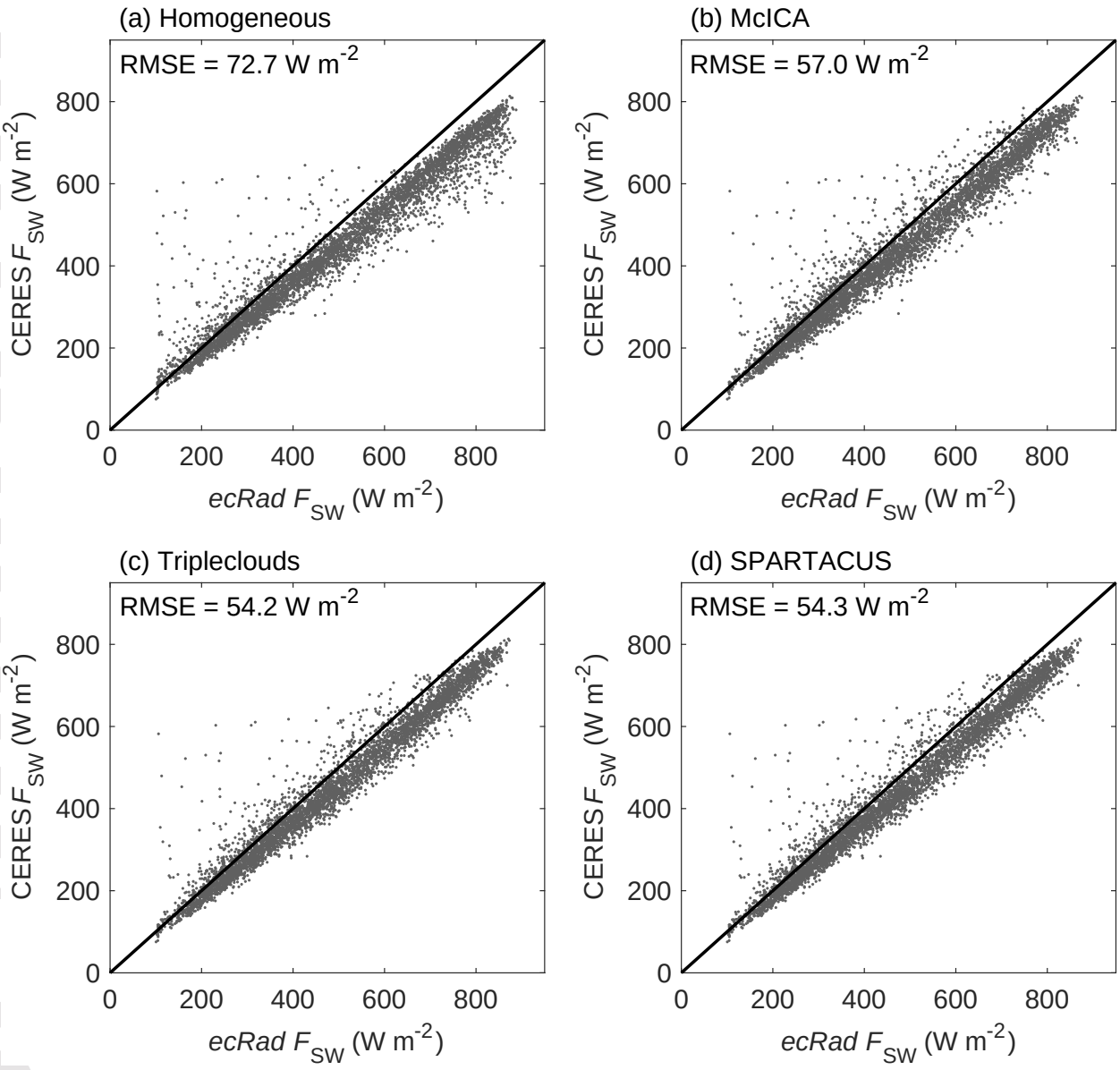


This article is protected by copyright. All rights reserved.

Author Manuscript



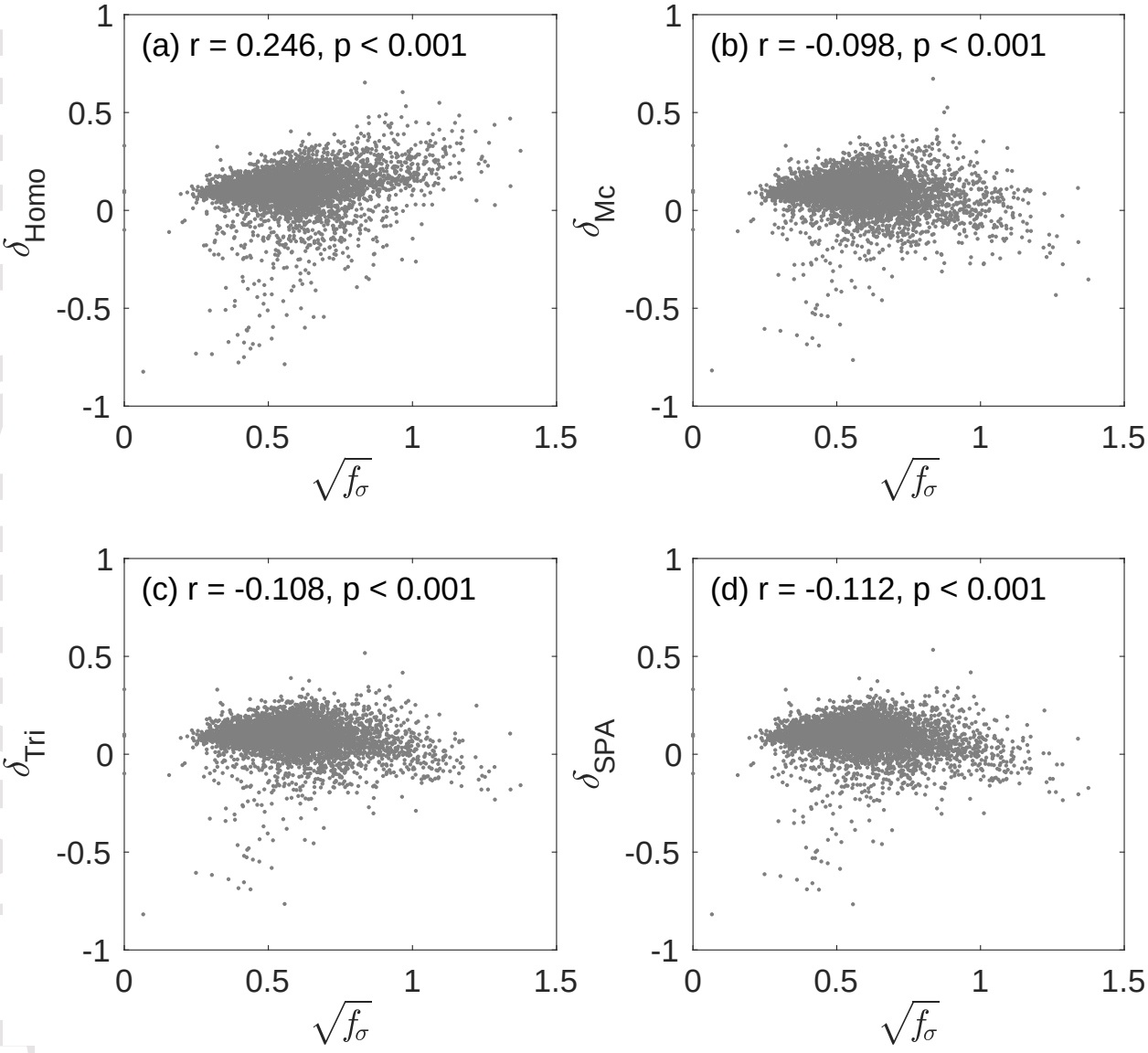
This article is protected by copyright. All rights reserved.



Author Manuscript

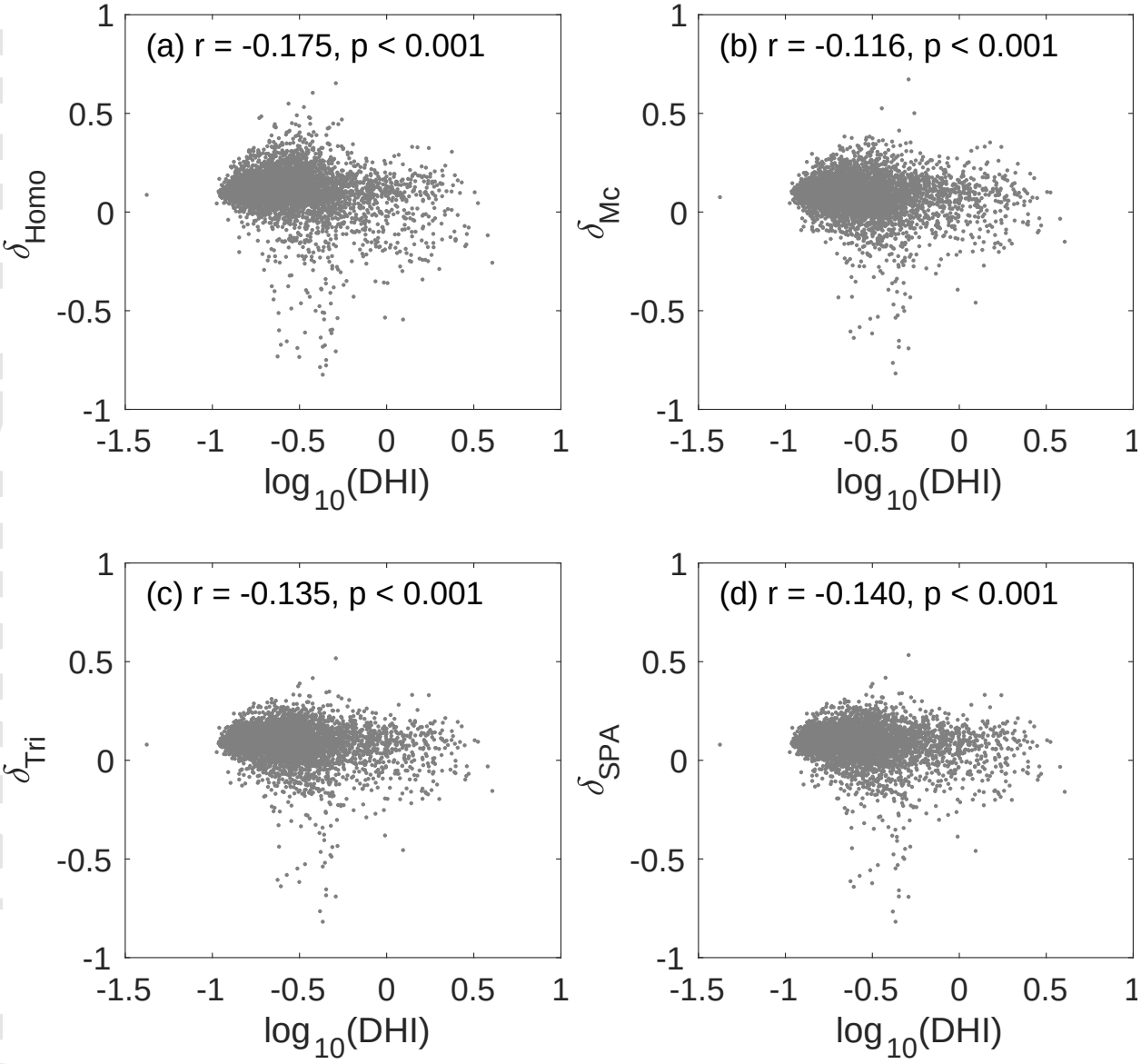
This article is protected by copyright. All rights reserved.

Author Manuscript



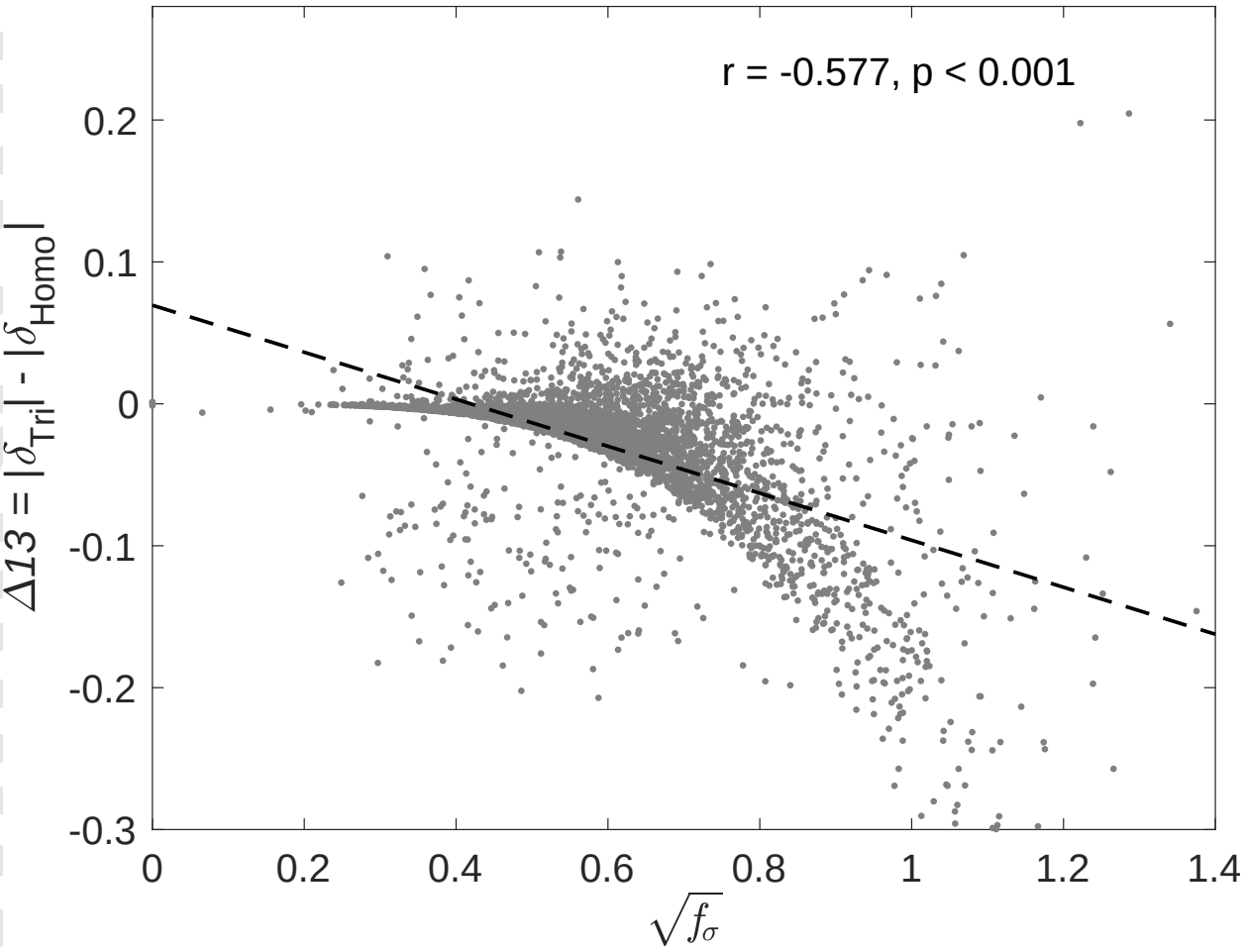
This article is protected by copyright. All rights reserved.

Author Manuscript



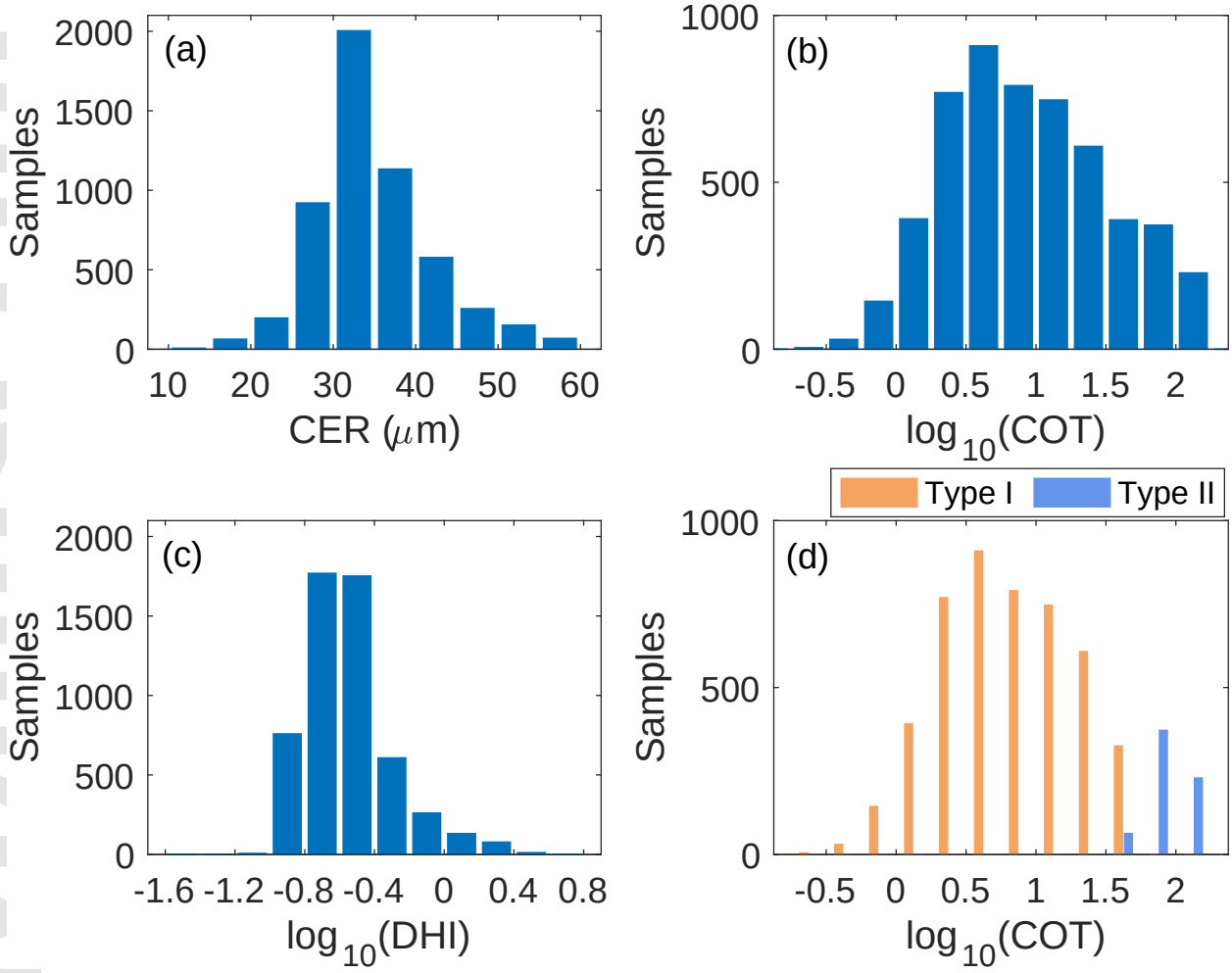
This article is protected by copyright. All rights reserved.

Author Manuscript



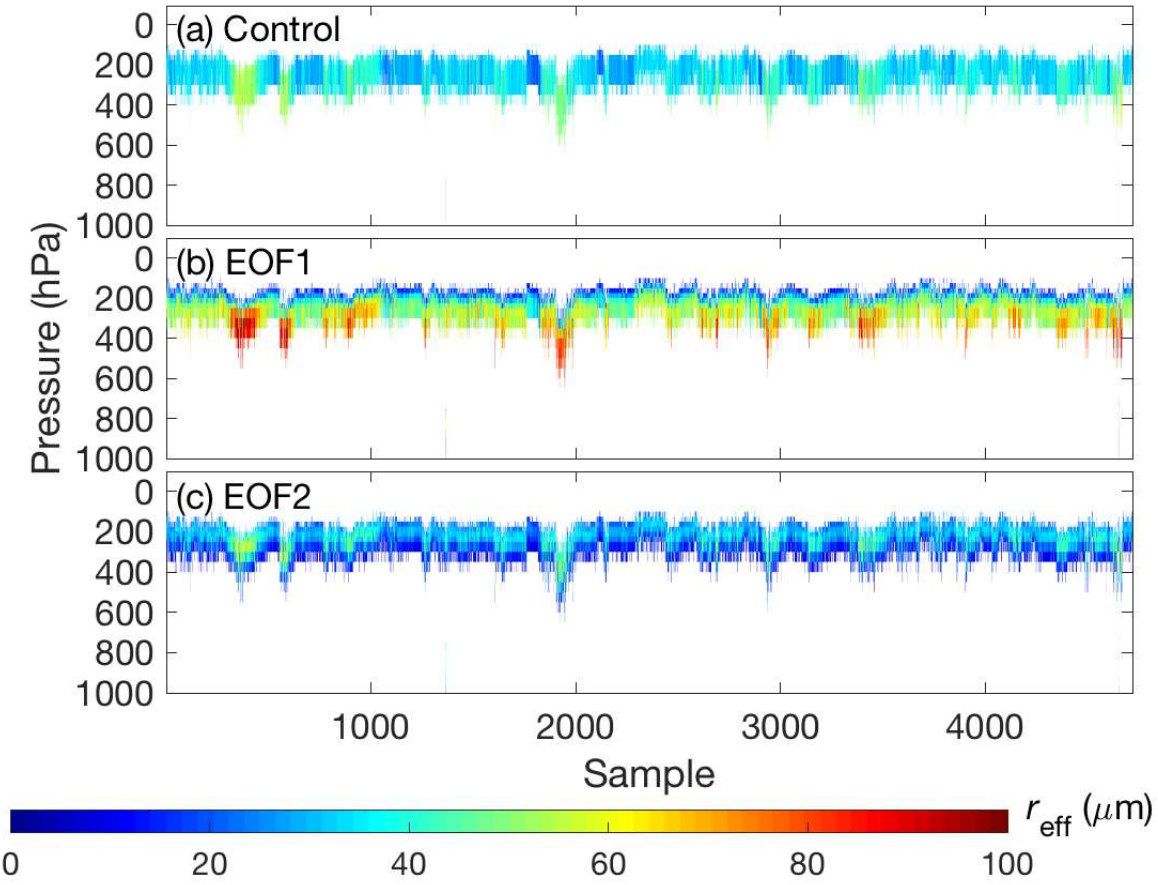
This article is protected by copyright. All rights reserved.

Author Manuscript

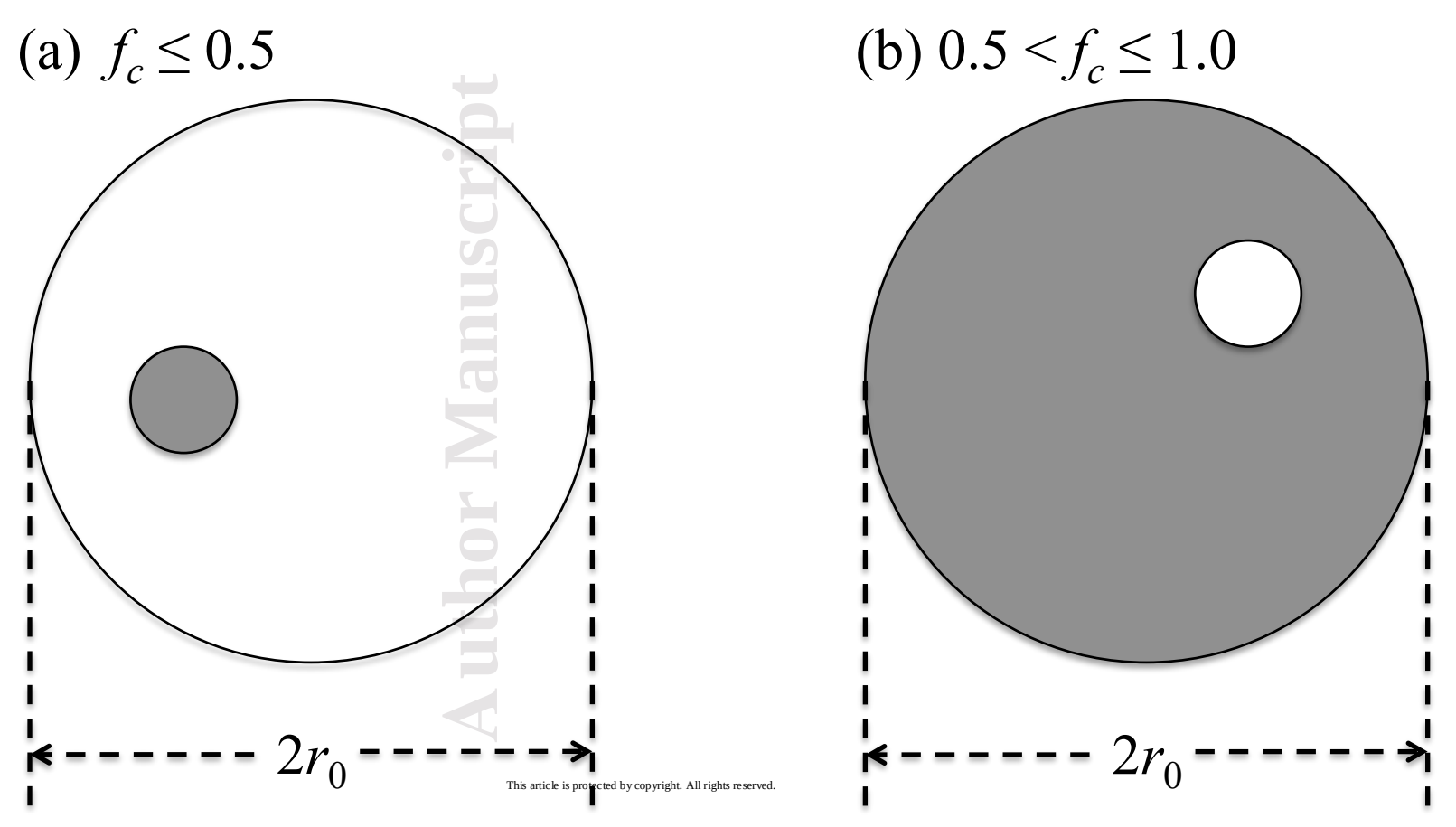


This article is protected by copyright. All rights reserved.

Author Manuscript



This article is protected by copyright. All rights reserved.



Author Manuscript

This article is protected by copyright. All rights reserved.